Quantitative plasma spectroscopy in a resistive shell reversed-field pinch

Anders Hedqvist

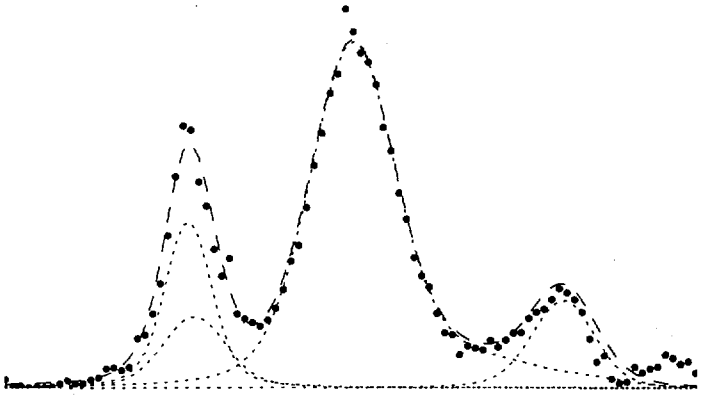

Department of Physics
Atomic and Molecular Physics
Royal Institute of Technology

Stockholm 1999

Quantitative plasma spectroscopy in a resistive shell reversed-field pinch

Anders Hedqvist

A thesis submitted in partial fulfillment
of the requirements for the degree of
Doctor of Philosophy
at the

Department of Physics
Royal Institute of Technology
Stockholm 1999

TRITA-FYS-1069
ISSN 0280-316X
Quantitative plasma spectroscopy in a resistive shell reversed-field pinch
Anders Hedqvist, 15 October 1999

KTH Högskoletryckeriet, Stockholm 1999

Please be aware that all of the Missing Pages in this document were originally blank pages

Quantitative plasma spectroscopy in a resistive shell reversed-field pinch

Anders Hedqvist

AKADEMISK AVHANDLING

som med tillstånd av Kungl Tekniska Högskolan framlägges till offentlig granskning för avläggande av teknologie doktorsexamen fredagen den 26 november 1999 kl 10.00 i Kollegiesalen, Administrationsbyggnaden, Kungl. Tekniska Högskolan, Valhallavägen 79, Stockholm.

Avhandlingen försvaras på engelska

Kungliga Tekniska Högskolan
Stockholm 1999

Hedqvist, Per Anders Wilhelm

Quantitative plasma spectroscopy in a resistive shell reversed-field pinch
(in English), Department of Physics, Atomic and Molecular Physics,
Royal Institute of Technology, Stockholm 1999

Abstract

The subject addressed in this thesis is quantitative plasma spectroscopy. Measurements of electron temperature and impurity ion density, performed at EXTRAP-T2, are aimed to investigate the effects of operating a reversed-field pinch with a resistive shell and a graphite wall. The spectroscopic measurements are analyzed with a collisional-radiative model and a consistency check is performed for the measurements and the model itself.

The resistive shell results in wall-locked modes, enhanced plasma-wall interaction and degraded confinement. Measurements of vacuum ultraviolet resonant transitions of carbon and oxygen show that the local heating of the wall, at the position of the locking, leads to influxes of hydrogen and impurities, resulting in a cold and resistive plasma. Effects on the local scale are also observed. Spatially-resolved measurements of line emission originating from charge exchange collisions are used to investigate the change in neutral hydrogen profile. Temporal correlations between soft x-ray emission and poloidal loop voltage at the position of the wall-locked modes are observed and in connection, a decrease in central electron temperature, indicating there is a direct energy loss channel between the center and the edge.

The hydrogen recycling properties of the graphite wall are investigated in an isotope exchange experiment. The density of the hydrogen isotopes are measured from spectral line emission and compared with recycling models.

In charge exchange collisions between fully stripped chlorine and thermal deuterium, observed in JET plasmas, only a single n-level is populated. This is different from most ions and may be used to test models for calculating charge exchange collision cross-sections.

Descriptors

Quantitative plasma spectroscopy, collisional-radiative model, VUV spectroscopy, EXTRAP-T2, reversed-field pinch, impurity content, resistive shell modes, power balance, charge exchange excitation, JET.

TRITA-FYS-1069 • ISSN 0280-316X

Hedqvist, Per Anders Wilhelm

Quantitative plasma spectroscopy in a resistive shell reversed-field pinch (in English), Department of Physics, Atomic and Molecular Physics, Royal Institute of Technology, Stockholm 1999

Abstract

The subject addressed in this thesis is quantitative plasma spectroscopy. Measurements of electron temperature and impurity ion density, performed at EXTRAP-T2, are aimed to investigate the effects of operating a reversed-field pinch with a resistive shell and a graphite wall. The spectroscopic measurements are analyzed with a collisional-radiative model and a consistency check is performed for the measurements and the model itself.

The resistive shell results in wall-locked modes, enhanced plasma-wall interaction and degraded confinement. Measurements of vacuum ultraviolet resonant transitions of carbon and oxygen show that the local heating of the wall, at the position of the locking, leads to influxes of hydrogen and impurities, resulting in a cold and resistive plasma. Effects on the local scale are also observed. Spatially-resolved measurements of line emission originating from charge exchange collisions are used to investigate the change in neutral hydrogen profile. Temporal correlations between soft x-ray emission and poloidal loop voltage at the position of the wall-locked modes are observed and in connection, a decrease in central electron temperature, indicating there is a direct energy loss channel between the center and the edge.

The hydrogen recycling properties of the graphite wall are investigated in an isotope exchange experiment. The density of the hydrogen isotopes are measured from spectral line emission and compared with recycling models.

In charge exchange collisions between fully stripped chlorine and thermal deuterium, observed in JET plasmas, only a single n-level is populated. This is different from most ions and may be used to test models for calculating charge exchange collision cross-sections.

Descriptors

Quantitative plasma spectroscopy, collisional-radiative model, VUV spectroscopy, EXTRAP-T2, reversed-field pinch, impurity content, resistive shell modes, power balance, charge exchange excitation, JET.

TRITA-FYS-1069 • ISSN 0280-316X

Preface

I think it all started during the course in atomic and molecular physics held by professor Peter Erman in the autumn of 1993. I was fascinated by the subject and decided that I wanted to do a PhD. I thought the best way was probably to do the Master of Science thesis at the same department and set off to talk with professor Erman. He suggested that I should do something in fusion plasma spectroscopy and directed me to professor Elisabeth Rachlew-Källne (I remember that I said that I didn't believe in plasmas of hundred of million degrees but Peter insisted, luckily). In the meeting with Elisabeth it was decided that I would do a project work on the EXTRAP-T1 experiment and if everything worked out, continue with a PhD. It worked out all right and I was given the opportunity to participate from the start of the new experiment, EXTRAP-T2.

I want to thank Elisabeth for this opportunity and also for the way that she has been supervising me. I have been given the possibility to find my way, try experiments and solutions on my own, and this is very important for me. But at the same time she has always been there with help, guidance and encouraging when needed (definitely needed from time to time). She has also taught me the perhaps most valuable thing during my PhD time. When experiments were not very successful (frequently, especially in the beginning) I went to Elisabeth and complained,'I have a problem'. The reply she gave was always the same,'No, there are no problems, only solutions'. That is absolutely positive thinking, to see solutions rather than problems, and a very important thing if you do research. And, being a Lennonist I directly understood what she was meant.

The work that has been done over the past six years has been shared with many people and I like to thank my and friends and colleagues in the spectroscopy group, Jerzy Brzozowski, Thieyacine Fall, Pontus Hörling and especially Jesper Sallander, with who a great deal of the work in this thesis has been done. Many thanks also to the guys in the control room, Gunnar

Hedin and David Larsson, for good collaboration and fun times even when the days were long and T2 was impossible.

Many thanks to the people at TFTR in Princeton and especially Alan Ramsey for everything during my short stay there in 1995. Equally many thanks to the people at JET for my stay there, Manfred von Hellermann and his group and especially Klaus-Dieter Zastrow, for the many interesting lunch discussions and Jakob Svensson for all the good times and the many interesting discussions on minds and music. And thank you Elisabeth, for making these trips possible.

A great part of my time has been spent at the Division of Fusion Plasma Physics at the Alfvén Laboratory and I want thank everyone there for the friendly atmosphere and always feeling being welcome. Special thanks to all who helped with physics and discussions and to the technical staff for all the help (with strange requests).

And many thanks to all colleagues and friends at the Department of Physics I. It is a relaxed and fun place with creative discussions (not necessary about physics) and happenings and this is important for the work. There will always be times when experiments are not working and feelings are low but I have always looked forward to go to work.

And finally, many thanks to my family for the nice collaboration and for being there for me.

Stockholm, October 15, 1999

Anders Hedqvist

Contents

List of papers

This thesis is based on the work presented in the following papers:

I. A. Hedqvist and E. Rachlew-Källne,
Time-resolved VUV spectroscopy in the EXTRAP-T2 reversed field pinch.
Plasma Physics and Controlled Fusion **40** 1597 (1998)

II. J. Sallander, A. Hedqvist and E. Rachlew-Källne,
Measurements of neutral hydrogen profiles on the EXTRAP-T2 reversed-field pinch from time-resolved C^{5+} line emission.
Journal of Physics B: Atomic, Molecular and Optical Physics **31** 3905 (1998)

III. S. Hokin, H. Bergsåker, P. Brunsell, J. Brzozowski, M. Cecconello, J. Drake, G. Hedin, A. Hedqvist, D. Larsson, A. Möller, E. Sallander and H.-E. Sätherblom,
Locked modes and plasma-wall interaction in a reversed-field pinch with a resistive shell and carbon first wall.
Proceedings of the 17th International Conference on Fusion Energy organized by the IAEA, Yokohama (1998)

IV. D. Larsson, H. Bergsåker and A. Hedqvist,
Hydrogen recycling in graphite at higher fluxes.
Journal of Nuclear Materials **266-269** 851 (1999)

V. E. Sallander, J. Sallander and A. Hedqvist,
Changes in transport and confinement in the EXTRAP-T2 reversed field pinch.
Plasma Physics and Controlled Fusion **41** 1179 (1999)

VI. A. Hedqvist and J. Sallander,
On the consistency of spectroscopic ion density measurements.
To appear in Plasma Physics and Controlled Fusion

VII. A. Hedqvist, M. O'Mullane, J. Nordquist, E. Rachlew-Källne and K.-D. Zastrow,
Contributions of thermal charge exchange excitation to the Rydberg series of Cl^{16+}.
Submitted to Journal of Physics B: Atomic, Molecular and Optical Physics

People asking questions,
lost in confusion.
Well, I tell them there's no problem,
only solutions.

John Lennon

Chapter 1

Introduction

The energy demand of the world will increase. Even though the energy used in the developed world is leveling out, the developing world will demand more energy as their standard of living will eventually increase. The world's population will also increase, with about 50% to nine billion people in the next 50 years. Acknowledging the problems with fossil fuel burning, e.g. exhausts of greenhouse gases and a limited supply, other means of energy production are needed as we look into the 21st century. Of all possibilities, nuclear fusion stands out as the most advantageous and possible the only one that could, if necessary, be the sole supplier of energy. A virtually clean energy source with an almost unlimited supply of fuel will be the reward when the first nuclear fusion power plant starts producing energy sometime in the middle of the next century.

1.1 Nuclear fusion

Nuclear fusion is the process that powers our sun and the stars. Light nuclei, e.g. hydrogen, are fused together to form a heavier nucleus. Several reactions are possible but the one that is easiest to achieve and therefore of main interest in fusion research is the reaction between the two isotopes of hydrogen, deuterium (D) and tritium (T). Together they form a helium (He) nuclei and a neutron (n) in the so-called D-T reaction,

$$D + T \rightarrow He + n + 17.6 \text{ MeV} \tag{1.1}$$

The two protons and the two neutrons that form the He nucleus are more tightly bound together than the nuclei of the hydrogen isotopes are

separately. This results in that the mass of the particles on the right side is less than the mass of the particles on the left side. It is this reduction in mass that is released as energy in the fusion process according to Einstein's famous formula,

$$E = mc^2 \tag{1.2}$$

In order to overcome the repulsive Coulomb force between the two positively charged particles and to fuse them together, a significant pressure has to be applied. This can be done with the gravitational force of a star, pressing the hydrogen nuclei together in the center, as it is done in our sun. It can also be done by heating the particles to very high temperatures. In order for the D-T reaction to be relevant in a fusion power plant the temperature has to be of the order of 150 million degrees. This is routinely done in the larger fusion experiments. In fact, temperatures as high as 450 million degrees, about 30 times the temperature in the center of the sun, has been reached. A scientific achievement in itself.

High temperature is a necessary but insufficient condition for fusion energy production. We also have to fulfill the so-called Lawson criterion [1],

$$n_{\mathrm{i}}\tau_{\mathrm{E}} > 10^{20} \quad [\mathrm{m}^{-3}\ \mathrm{s}] \tag{1.3}$$

which states that we need, at the same time, a sufficiently high ion density, n_{i}, and to confine the energy for a sufficient long time, τ_{E}, to produce more energy than what is lost through radiation.

There are two principal ways to do this. In inertial confinement [2, 3] a very high density but low confinement time is obtained by applying very intensive laser light to small pellets of frozen deuterium and tritium. In magnetic confinement the density is low but the confinement time is long. This is achieved by confining the charged particles to a closed volume with the use of magnetic fields.

So far, the way to fusion energy through magnetic confinement has been the most successful one. It has shown reactor relevant conditions and is most likely to be the first, but perhaps later on not the only way to produce fusion energy.

1.2 Magnetic confinement

When a gas is heated to approximately 10000 degrees ($\sim$ 1 eV) the energy is sufficient to remove a bound electron from an atom and thereby ionizing

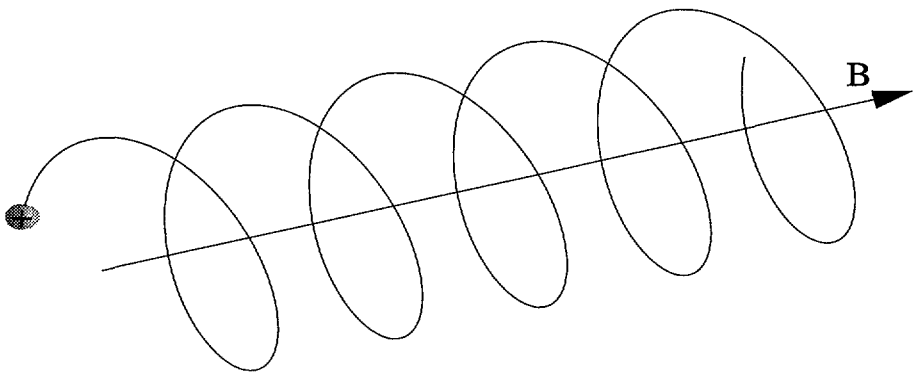

Figure 1.1. A positively charged particle, spiraling around the magnetic field line under the influence of the Lorentz force (picture from [5]).

it. We now have a plasma [4], a quasi-neutral[1] gas containing electrons, ions and neutral atoms and molecules. The hot plasma has to be kept away from contact with any surrounding material or it will be cooled down and destroyed. The plasma can be kept in place, or confined, with the use of magnetic fields. Particles, with charge q, spiral around the magnetic field lines $\mathbf{B}$ with a velocity $\mathbf{v}$ under the influence of the Lorentz force $\mathbf{F}$,

$$\mathbf{F} = q\mathbf{v} \times \mathbf{B} \tag{1.4}$$

The base for almost all magnetic field configurations for confining plasmas is the screw pinch that has been bent into a torus (a doughnut) to avoid losses at the ends. The magnetic field consists of primarily two parts, a toroidal magnetic field that goes the long way around the torus and a poloidal magnetic field that goes the short way around. The resulting magnetic field makes a screw around the torus.

The fusion research is focused on three different magnetic field configurations, the tokamak, the stellarator and the reversed-field pinch.

[1] Quasi-neutral: there are equal amount of negative charges (electrons) and positive charges (ions) in a sufficiently large volume.

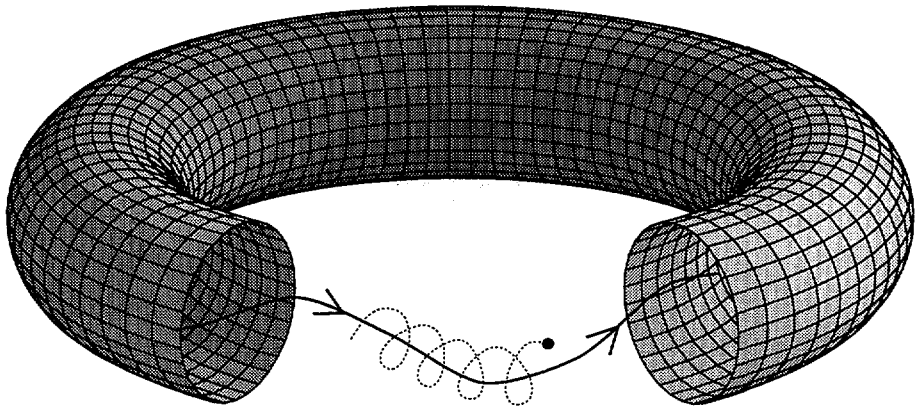

Figure 1.2. The helical magnetic field in a screw pinch bent into the form of a torus. This is the base for the virtually all magnetic field configurations (picture from [6]).

1.2.1 The tokamak and the stellarator

The tokamak [7] is to date the most successful magnetic field configuration in fusion experiments. The toroidal magnetic field is set up with a series of toroidal field coils, which are current-carrying loops in the poloidal direction. The toroidal magnetic field is strong, several teslas. The poloidal magnetic field is produced by the toroidal current which in turn is induced in the plasma with a transformer. The plasma acts here as the secondary winding of the transformer. The poloidal field is about 1/10 of the toroidal magnetic field.

The tokamak has shown reactor relevant conditions for ion temperature, ion density and energy confinement time but not all at the same time. The world's largest fusion experiment, the JET Joint Undertaking tokamak, has reached Q=1 which means that the fusion power produced exactly balance the power losses. The plasma will ignite at Q=5 (ideally) when the power in the fusion produced α-particles (helium nucleus) will balance the losses and keep the reaction going. This state is also called a burning plasma as it keeps on by itself and only fuel is needed to add.

If the Lawson criterion (equation 1.3) is multiplied with the ion temperature we get the so-called triple product and it is about 10 times the Lawson criteria for ignition. Since 1955, when nuclear fusion started as a way of

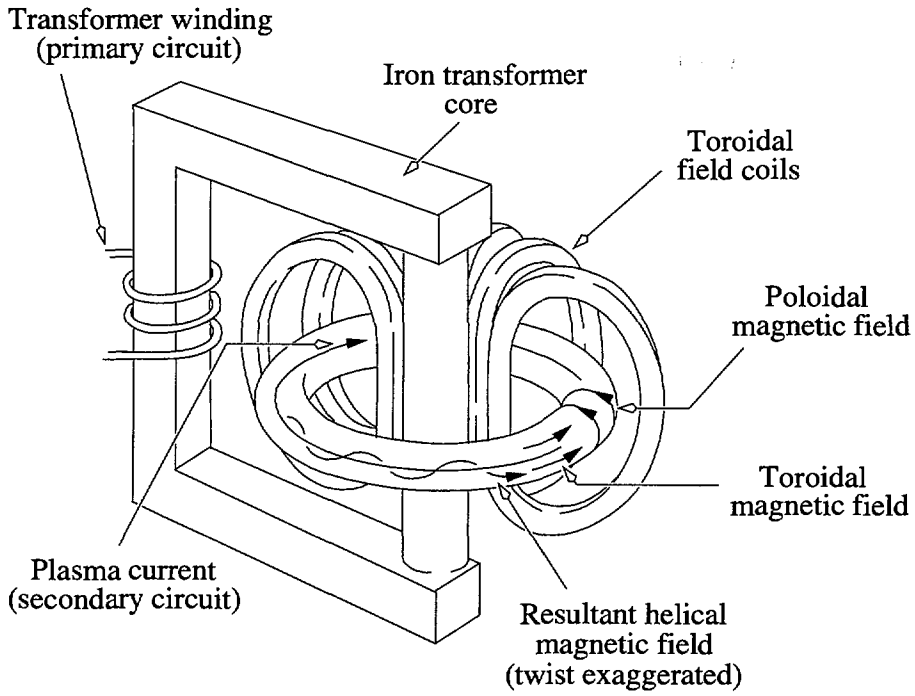

Figure 1.3. A schematic picture of a tokamak. Also applicable for the reversed-field pinch although the toroidal fields coils are much smaller then (picture from [8]).

producing energy in a controlled fashion, the triple product has improved almost eight orders of magnitude. Left is only a small step, a factor of five to reach the requirements of a burning plasma. The first fusion experiment to reach ignition is most likely to be based on the tokamak concept.

As the tokamak has very fine properties and is a robust configuration, it also has its drawbacks. The ratio between the plasma pressure and the magnetic pressure, the β-value, is low. This means that large magnetic fields are used to confine low plasma pressures and hence the efficiency of fusion power production will be low. Since magnetic field strength is expensive, the tokamak might experience that producing fusion energy was not the difficult part but to do it in an economically feasible way.

One of the problems with the operation of a tokamak is that it uses a strong toroidal current to produce the poloidal field. The current can drive

instabilities which can lead to a disruption of the plasma discharge. An event like that in a fusion reactor where the energy stored in the plasma will be great, can cause significant damage to the reactor. One solution to this problem is the stellarator [9]. In this magnetic field configuration, there is no toroidal current. Both the toroidal and the poloidal magnetic fields are produced by coils. These coils have a complicated shape and they are designed with the aid of computers. The high requirements on the coils in order for them to produce the desired magnetic fields make them expensive to produce.

The stellarator performs on the level of tokamaks of similar size but they are not big enough to compare with front line of tokamak experiments. The next generation of stellarators [10] will hopefully show that they are ready to match the tokamak in performance.

1.2.2 The reversed-field pinch

The reversed-field pinch (RFP) [11] has more in common with the tokamak than with the stellarator. The poloidal magnetic field is induced by the toroidal current, just like in a tokamak. The toroidal magnetic field, which is similar in strength to the poloidal field, is by large produced by the plasma itself through a process called the RFP dynamo. In this process, toroidal current in the center is converted into poloidal current at the edge, which in turn produces the toroidal field. By this self-organization, the plasma enters a near-minimum energy state [12]. A consequence of this state is that the toroidal magnetic field must change direction at the edge. This field-reversal is responsible for the name of the configuration. There are several models for calculating the magnetic fields and current densities, e.g. the polynomial function model (PFM) [13] and the result of this is shown in figure 1.4.

Since the plasma itself sets up the magnetic field configuration, the balance between the poloidal and toroidal magnetic fields stays the same. In principle this means that the RFP plasma can be heated to ignition by only increasing the plasma current. Another consequence of the fact that the plasma produces the necessary toroidal magnetic field, is that no big and expensive toroidal field coils are needed and that the reversed-field pinch offers the possibility of a compact and economical reactor. A serious drawback is that the dynamo works with the use of magnetic fluctuations and this is a strong source of transport and thereby losses of particles and energy [14, 15].

The reversed-field pinch is normally run with a conducting shell. On

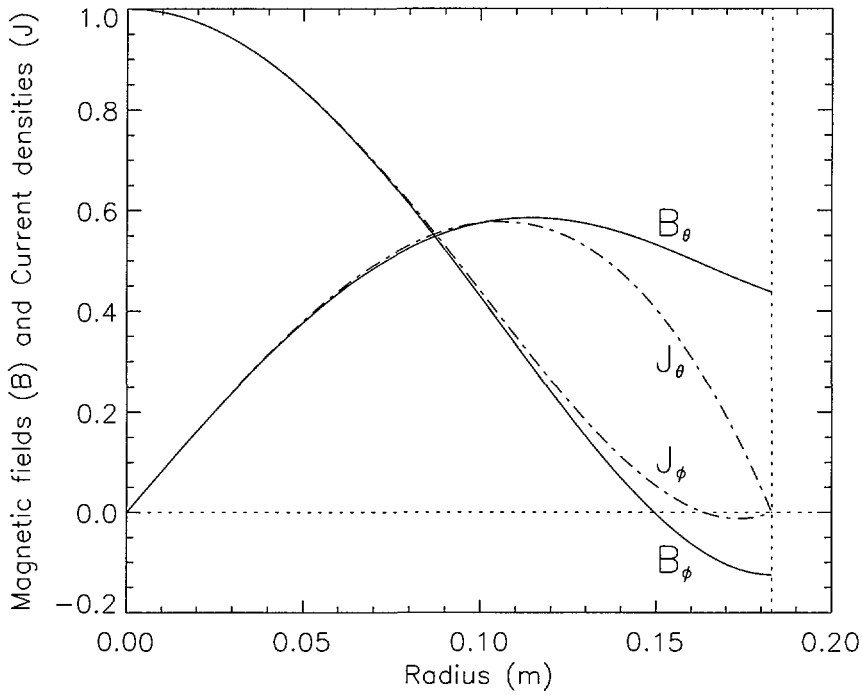

Figure 1.4. Normalized magnetic fields and current densities in a reversed-field pinch with dimensions (minor radius) of EXTRAP-T2. The poloidal direction, or the short way around (see figure 1.3) is denoted θ while the toroidal direction, or the long way around, is denoted ϕ. Note that the toroidal magnetic field changes direction at a radius of 0.15 m.

the time-scale of a discharge the shell will work as a perfect conductor and prevent the magnetic field from penetrating. This is used for stabilizing the outward drift of the plasma column. The shell is also used to prevent certain magnetic field perturbations, or modes, to appear. The two leading RFP experiments, MST [16] at Madison, Wisconsin, USA and the worlds largest RFP, the RFX [17] at Padua, Italy, both operate with conducting shell. So far, the RFP has not performed on the level of tokamaks of the same size and current. Perhaps the new experiment in Japan, the TPE-RX [18], can show that the RFP has a future as a reactor relevant concept.

One thing that must be investigated is operation with a resistive shell. As

the duration of the plasma discharge gets longer, as it eventually must be if the RFP ever will work as a reactor, no material will be perfectly conducting and hence the magnetic field may slowly slip through the shell. EXTRAP-T2 [19] was supplied with a resistive shell to investigate this effect. The result is the presence of so-called wall-locked modes [20] which are magnetic field perturbations that have a degrading effect on confinement. A solution to this might be a shell that is conducting on the time-scale for these modes but resistive on the time-scale of a plasma discharge. This will be the objective for the rebuilt EXTRAP-T2 which will start operation sometime in the beginning of the next year.

1.3 Spectroscopy

What is the density and temperature of our plasma? How long do we confine the particles and the energy? These are questions that we need to answer to see if we make any progress in reaching (and eventually exceeding) the Lawson criterion. It is also information that we need in order to understand the basic behaviour of the plasma.

Spectroscopy [21, 22] gives a wonderful tool to investigate these and other properties of the plasma. The light emitted by the plasma can, with the use of atomic and molecular physics, be used to diagnose the plasma. Our plasma contains electrons and ions as well as neutral atoms and molecules, although the charged particles dominates. Most of these particles come from hydrogen but there are always other species present, so-called impurities, that come from the wall that surrounds the plasma. Carbon, oxygen and metals are normal impurities and even though they are only a few percent of the plasma density they are very important.

In collisions between electrons and ions, the electron may give some of its kinetic energy to the ion. The ion may be ionized if the energy is sufficient and release a bound electron,

$$A^z + e^- \rightarrow A^{z+1} + e^- + e^- \tag{1.5}$$

It may also be excited where a bound electron is lifted to a higher energy state (still bound to the ion). For most excited states the electron will return very quickly to lowest energy state that is available. The difference in energy between these two bound states can be released in the form of a photon,

$$A^z + e^- \rightarrow (A^z)^* + e^- \rightarrow A^z + e^- + h\nu \tag{1.6}$$

The energy states of an ion or atom are fixed (at least to a first approximation). This means that the photon that is emitted when an electron goes from a higher energy state to a lower will have energy, and hence wavelength, according to the transition. This leads to that the emission spectrum from the plasma will show sharp peaks at these wavelengths. These wavelengths are also (more or less) unique for a given ion. A spectrum will therefore tell what species the plasma contains, and a detailed analysis can answer a number of questions regarding the status of the plasma.

The emission that comes from transitions between bound energy states of an ion is called line emission and is the foundation of virtually all spectroscopy work. For an ion to emit this line emission it needs to have at least one bound electron left. In order to ionize hydrogen and remove its only electron, 13.6 eV is needed. In a plasma where the temperature is much higher, all hydrogen will be ionized except near the plasma boundary where the temperature is low enough. If our plasma would be perfectly clean and containing only hydrogen we would only detect line emission from the edge of the plasma and without any means to say what goes on in the center. The rescue for the spectroscopist is impurities. These species have more electrons and require more energy to be fully ionized. This means that we will have line emission even from the hottest part of the plasma and this is the reason why almost every spectroscopy work is based on impurities.

The intensity[2] of a spectral line with respect to wavelength depends on several parameters,

$$I(\lambda) = I(n_\mathrm{i}, n_\mathrm{e}, T_\mathrm{i}, T_\mathrm{e}, v, E, B) \tag{1.7}$$

The wavelength position of a spectral line depends on the velocity v of the ion. If the emitting ion is moving towards the receiver, or where the recording of the signal is done, the emitted light is Doppler shifted towards shorter wavelength (higher frequency) and opposite if the ion is moving away. If there is no preferred direction for the motion for an assembly of particles, the Doppler shift will be both to longer and shorter wavelengths resulting in a broadening of the spectral line. In a plasma, the thermal motion of the ions is random in direction and therefore results in a broadening of the spectral line. This means that the temperature of the ions, T_i, can be calculated by measuring the width of a spectral line. The influence of electric (E) and magnetic (M) fields on spectral line emission is more complicated. They shift the energy levels of the atom by the Stark and

[2]Normally given in units of Photons $\mathrm{m}^{-3}\ \mathrm{sr}^{-1}\ \mathrm{s}^{-1}\ \text{Å}^{-1}$.

Zeeman effect, respectively. These effects are normally negligible in low density fusion plasmas.

The integral over $I(\lambda)$ with respect to wavelength gives the intensity of a spectral line,

$$I = \int I(\lambda) d\lambda \tag{1.8}$$

and it depends on the electron density n_e, the ion density n_i and the electron temperature T_e. Excitation is caused by collisions between electrons and ions. If we double the electron density or the ion density we will have twice as many collisions and thereby twice as many excitations and emitted photons. The probability per unit time that a collision actually leads to an excitation of a specific level is called the rate coefficient, $\langle \sigma v \rangle$[3] This quantity is strongly dependent on electron temperature and weakly on electron density. The electron temperature is the average kinetic energy of the electrons in the plasma. The dependence on electron temperature in the rate coefficient comes from that the colliding electron has to have enough energy to give to the ion to excite it. The higher the temperature, the more electrons will have enough energy to excite. If we put all this dependences together we end up with a very useful formula,

$$I = n_i n_e \langle \sigma v \rangle \tag{1.9}$$

The electron density is usually measured with other techniques than spectroscopy. If we measure the intensity I of spectral lines we can deduce the density of different impurity ions and also the electron temperature. If we know the densities of the different ions in the plasma we can calculate the average ion charge, Z_{eff},

$$Z_{\text{eff}} = \frac{\sum Z_i^2 n_i}{\sum Z_i n_i} \tag{1.10}$$

This number tells us how clean (or dirty) our plasma is. A pure hydrogen plasma has Z_{eff} equals to one and if it would be contaminated with carbon Z_{eff} would eventually reach six, if the electron temperature and the carbon density are sufficiently high. In most fusion plasmas, Z_{eff} is between 1.5 and 3.0. This number is of crucial importance in a fusion reactor. In order produce fusion power the energy produced must exceed the energy lost by

[3]Also denoted q. Normally given in units of m^3s^{-1}.

radiation. A fusion plasma of Z_{eff} of 2.0 will have twice the radiation losses of a pure hydrogen plasma.

Chapter 2

Quantitative plasma spectroscopy

The aim of quantitative plasma spectroscopy is to use the light emitted by the plasma to determine quantities such as temperature and density. The way to do it consists of three parts, the measurement of the light, the calibration of the detecting system and finally the model for the interpretation of the collected data.

2.1 The measurement

An advantage of plasma spectroscopy is that it uses light that is emitted by the plasma. There are no perturbations to the plasma although some "RFP physicists" might say that the port holes in the vacuum vessel through which the signal is collected is one. The light is integrated along a line of sight through the plasma,

$$I(\lambda, t) = \int I(\lambda, t, r) dr \tag{2.1}$$

This is the one limiting factor of spectroscopy; the loss of spatial information. It can be helped by reconstructing the spatial dependence by viewing the plasma in different directions, e.g. tomography. In some cases, the light that is of interest is created along a line, e.g. laser photons scattered by electrons in Thomson scattering setup. By recording the signal perpendicular to the line, only the light at the intersection will be recorded. A true spatially resolved measurement but slightly perturbative.

The detecting equipment can be a wavelength dispersive system, such as a spectrometer or a monochromator. It is more or less the same instrument. The spectrometer images the dispersed light onto a multichannel detector, such as an optical multichannel analyzer (OMA) or charged coupled device (CCD). With this arrangement we get a wavelength resolved image of the light. A monochromator on the other hand images the dispersed light onto a narrow exit slit, extracting a single wavelength. In this case the the detector is usually a fast time-responding device such as a photomultiplier (PM) tube.

Instead of a grating or a crystal as a dispersive unit, a wavelength sensitive filter can also be used. It is not as flexible as a monochromator but sometimes more suitable. In the visible wavelength region, the system usually consists of an interference filter that only transmits light of a narrow bandwidth, on the order of 10 Å, followed by a PM-tube. This kind of system is easy to work with and is much more sensitive to radiation than a monochromator. It is preferentially used for detecting weak bremsstrahlung radiation or fixed standard signal as H_α. In the x-ray wavelength region the filter usually is a thin metallic foil that blocks out light below a certain energy threshold. The detector can be a surface barrier diode (SBD). It is a simple setup for recording light in a wavelength region which otherwise makes a measurement difficult.

2.2 The calibration

Before any quantitative work may begin, the detection system and thereby the recorded signal has to be calibrated. A system can be calibrated with respect to wavelength or intensity. The latter case is normally divided into relative and absolute calibration. A relative calibration can only say that signal A is twice as strong as signal B whereas an absolute calibration will put absolute numbers to signal A and B[1].

Absolute calibration in the visible and ultraviolet (UV), near-visible wavelength region is easy done with a calibration standard tungsten lamp or a discharge deuterium lamp[2]. For shorter wavelengths such as vacuum ultraviolet (VUV) there is no small, table-top calibration source. Instead it is usually done by using the branching ratio technique [23]. It uses the fact that that transitions originating from the same upper level have a fixed intensity relation. If one transition is in the visible wavelength region, it may

[1]Normally given in units of Photons m^{-2} sr^{-1} $s^{-1}Å^{-1}$.

[2]Down to about 2000 Å where absorption in air becomes a problem.

be calibrated with the standard source. Since the intensity ratio is fixed the calibration can be transfered to the measured VUV transition. It is in principle possible to continue and to calibrate the x-ray region with this technique but it is more difficult to find connected lines for this purpose. Continuum bremsstrahlung may also be used, once it is measured in one wavelength range it is possible to calculate how much there will be in another range by simply changing the wavelength. It is more difficult because of the weak bremsstrahlung but on the other hand allows a calibration over many wavelengths [24].

Wavelength calibration is normally performed with a gas-discharge lamp containing for instance mercury or neon. Since the spectra of these species are well-known, recorded spectrum is compared to tabulated wavelengths of spectral lines. Outside the visible or UV range this is difficult and other methods must be used. One way is to use the light emitted by the plasma. If the detection system is well known so that the wavelength scale is known at least roughly, spectral line emission from the plasma can be used to get a more precis reading of the wavelength scale.

2.3 The model

One basic assumption in order to do quantitative spectroscopy on emitted light is that every photon, that is emitted along the line of sight in the direction of the observer, is recorded and not reabsorbed by the plasma. If this is true the plasma is said to be optically thin and that the optical depth, τ, is less than unity [25],

$$\tau = 5.4 \times 10^{-9} \lambda n l \sqrt{\frac{\mu}{T}} \tag{2.2}$$

where n is the density of the emitting/absorbing ions, λ is the wavelength of a (resonant) transition, l is the path length through the plasma, μ is the ion mass divided by the proton mass and T is the ion temperature. As an example, the numbers of interest for the $1s^2 2s\ ^2S - 1s^2 2p\ ^2P$ 1033.8 Å transition in O^{5+} is; μ is 16, n is typically 2.0×10^{11} cm^{-3}, the maximum length of the plasma volume is 36.6 cm and we can assume a temperature of 100 eV. With this, the optical depth is 0.16, i.e. the plasma is optically thin and we can disregard the problem of reabsorption.

The intensity of a spectral line depends on the number density of the excited state n^*,

$$I = n^* A \tag{2.3}$$

where A is the radiative transition probability. The objective of the model is to find an expression for the excited level population. The base is the so-called collisional-radiative model. Here, the ions are excited by collisions with electrons and de-excites by emitting a photon. The decay time of an excited state is usually much shorter than the collision time. This leads to that the density of excited states is low in comparison with the ground state and that virtually all collisions involve ions in the lowest energy state. The exception to this is the existence of metastable states. From these states there are no allowed transitions to the ground state. This means that the metastable states can exist for a much longer time than other excited states, even longer than the collision time and therefore has to be treated explicitly.

The rate equation for a state i that belong to an ion of charge z is given by,

$$\begin{aligned}
\frac{dn_{z,i}}{dt} &= \sum_j n_{z,j}(A_{ji} + n_e q_{ji}(T_e, n_e)) - \sum_j n_{z,i}(A_{ij} + n_e q_{ij}(T_e, n_e)) \\
&+ \sum_k n_{z+1,k} n_e \alpha_{z+1,ki}(T_e, n_e) - \sum_k n_{z,i} n_e \alpha_{z,ik}(T_e, n_e) \\
&+ \sum_k n_{z-1,k} n_e S_{z-1,ki}(T_e, n_e) - \sum_k n_{z,i} n_e S_{z,ik}(T_e, n_e) \\
&+ \sum_k n_{z+1,k} n_H C_{z+1,ki}(T_e, n_e) - \sum_k n_{z,i} n_H C_{z,ik}(T_e, n_e)
\end{aligned} \tag{2.4}$$

where A_{ij} is the radiative transition probability from state i to state j, $q_{ij}(T_e, n_e)$ is the electron collision rate coefficient, which is a function of both electron temperature T_e and electron density n_e. S and α are the ionization and recombination rate coefficients, respectively and finally C is the charge exchange rate coefficient. A perhaps easier way is to say that the first line of equation 2.4 is excitation and de-excitation, the second is recombination, the third is ionization and the last is charge exchange recombination.

If, and this is normally the case, the radiative decay time is much shorter than the collision time, virtually all collision processes involve an ion in the lowest energy state. The ionization and recombination terms in equation 2.4 may be regarded as a source term for the ground state from which the excitation takes place.

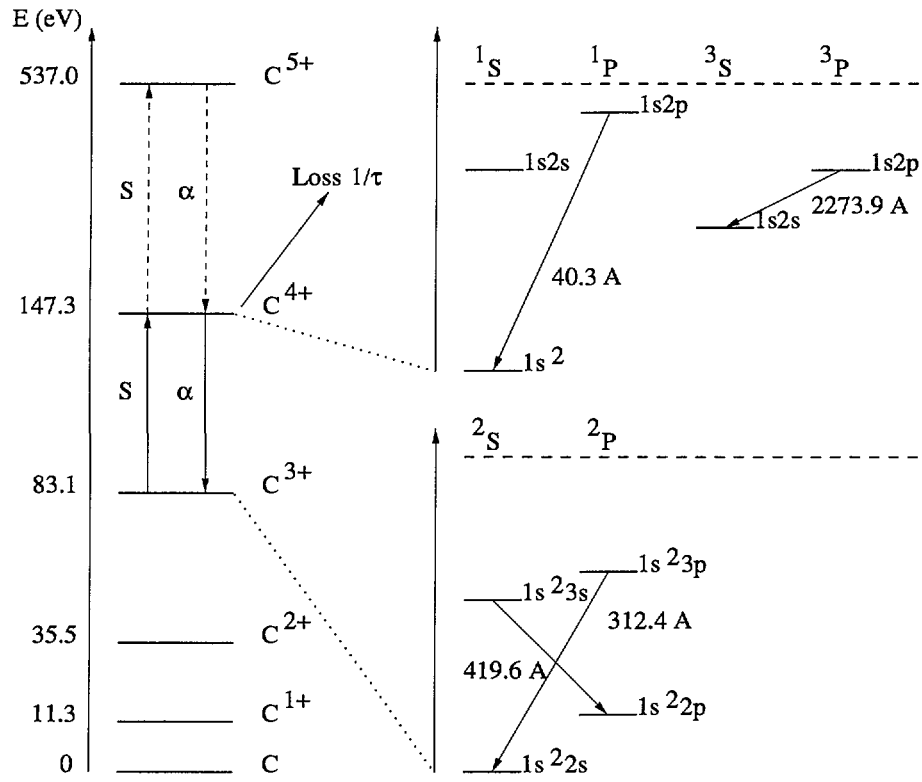

Figure 2.1. Ionization and excitation balance for carbon. The ionization balance is to the left. As an example the part that goes into calculating the C^{4+} ion density as described in paper I is shown. The processes that are included are marked with full arrows while the ones not included are represented by broken arrows. To the right are the excitation balances for C^{3+} and C^{4+}. Here the transitions that are used to calculate the respective ion densities are indicated. Included is also the resonant transition with the longest wavelength in C^{4+} (40.3 Å).

Because of this the rate equation is sometimes divided into two parts, the ionization and the excitation balance, shown in figure 2.1. The ionization balance deals with the density of the ground state and metastable states of every ionization stage while the excitation balance determines the excited state population. There are however exceptions to this view, e.g. the effect of charge exchange between neutral hydrogen and highly charged ions. This process preferentially populates a few high n-states. This process may under

certain circumstances be more dominant than the electron collision excitation from the ground state. An example of this is n=8 to n=7 transition in C^{5+}, which is studied in detail in paper II. At an electron temperature of some 100 eV, which is normal in EXTRAP-T2, the excitation rate coefficient is much lower than the rate coefficient for charge exchange excitation. At times of high neutral hydrogen density (at the plasma edge), charge exchange may be the dominating process. Under these circumstances, the charge exchange must be included in the excitation balance.

At steady-state, e.g. $dn/dt = 0$, the excitation balance will look as,

$$\frac{dn_{z,i}}{dt} = n_{z,1} n_e q_{1i} - n_{z,i} \sum A_{ij} = 0 \tag{2.5}$$

$$n_{z,i} = \frac{n_{z,1} n_e q_{1i}}{\sum A_{ij}} \tag{2.6}$$

where $n_{z,1}$ denotes the ground state density of ion of charged z. With equation 2.3 we get the intensity of a transition, between the states i and j, induced by electron collision excitation,

$$I = n_z n_e q_{ij}(T_e, n_e) \frac{A_{ij}}{\sum A_{ij}} \tag{2.7}$$

here the ion density n_z is the ground state density and is the one that appears in the calculations. Cascading effect from higher states to state i will occur and will enhance the intensity I. This effect is usually included in an effective rate coefficient for electron excitation from the ground state.

Equation 2.7 is the heart of the spectroscopy work in this thesis. If we take the ratio of two measured spectral lines belonging to the same ion, the densities cancel and we get something which is a function of electron temperature and density. If one of these quantities is known from some other measurement, the other may be deduced from this ratio. At EXTRAP-T2 this technique has been used to calculated the electron temperature. If we measure the intensity of a spectral line, and know the electron density and temperature and the rate coefficient, including the probability for radiative decay we can calculate the ion density. At first it might seem like we need to know a lot in order to determine the ion density but in reality that is not the case. Both electron temperature and density is what one might call standard diagnostics at a fusion experiment and therefore normally accessible data. The excitation rate coefficient and radiative decay probability have been calculated and measured for a long time and they are well-documented now.

If we now look at the ionization balance it can be written as,

$$\begin{aligned}\frac{dn_z}{dt} &= n_{z+1}n_e\alpha_{z+1,z} - n_z n_e S_{z,z+1} \\ &+ n_{z-1}n_e S_{z-1,z} - n_z n_e \alpha_{z,z-1} \\ &+ \sigma - n_z/\tau_p \end{aligned} \tag{2.8}$$

here the charge exchange part has been excluded as it has little importance in most cases. However, two terms have been added and they are the result of finite confinement of the particles due to transport and the interaction between the plasma and the surrounding wall. The first is a source term, σ, which is the influx at the edge of neutral particles. The second term is the loss of particles with the characteristic time, τ_p, the particle confinement time.

Neutrals enter the plasma. On their way towards the center they undergo collisions, get excited and ionized and finally lost on the time scale of the particle confinement time. Because of the finite confinement time, the ions do not reach as high ionization stage as they otherwise would have. Recombination has no effect on this balance as the particles search upwards among the ionization stages. At the plasma boundary, at steady-state, there is a balance between the influx of neutrals and ionization. The ionization balance now looks like,

$$\sigma = n_z n_e S_{z,z+1} \tag{2.9}$$

If this equation is divided with the intensity of a spectral line, given by equation 2.7, we get a source term divided by intensity equals the excitation rate coefficient divided by the ionization rate. The latter quantity is called ionization per photon and may be used to calculated the influx Γ_H of neutral hydrogen from the intensity of a hydrogen line, normally the H_α line. This in turn may be used to calculate the particle confinement time, τ_p,

$$\tau_p = \frac{\int n_p dV}{\int \Gamma_H dA} \tag{2.10}$$

where n_p is the proton density and where the integrals are performed over the plasma volume and surface, respectively.

In the interior of the plasma a similar ionization balance, as for neutrals at the edge, exists for highly charged ions. Here the balance is between ionization and loss due to the finite particle confinement time,

$$\frac{n_z}{\tau_p} = n_{z-1} n_e S_{z-1,z} \tag{2.11}$$

With the electron temperatures and densities present in EXTRAP-T2, the time to open the innermost closed shell of carbon or oxygen is much longer than the particle confinement time. This means that the helium-like ionization stage may in many cases be regarded as the final one. In the calculations of the ion densities described in paper I, the recombination term was included although it is of little importance. With this the density of He-like ions may be expressed in terms of the Li-like ion density,

$$n_{He} = \frac{n_{Li} n_e S_{Li \to He}}{1/\tau_p + n_e \alpha_{Li \to He}} \tag{2.12}$$

The predictions from this model are further studied in paper VI.

Chapter 3

EXTRAP-T2 and JET

The work presented in this thesis has been performed at two different fusion experiments, the EXTRAP-T2 reversed-field pinch, located at the Alfvén Laboratory in Stockholm, Sweden and the worlds largest fusion device, the JET Joint Undertaking, at Culham, United Kingdom.

3.1 EXTRAP-T2

EXTRAP-T2 is a medium-sized reversed-field pinch. It has a major radius R of 1.24 m and a minor radius a of 0.183 m. It is a continuation of the OHTE experiment [26] that was run at General Atomics in San Diego, USA.

There are two aspects of EXTRAP-T2 that influence the performance more than anything else. The first is that it has a resistive shell. This is different from most RFP experiments that usually operates with a conducting shell. A (perfectly) conducting shell will prevent the magnetic field from penetrating the shell. This is used to balance the outward drift of the plasma column and also to suppress the growth of magnetic modes and instabilities. However no material work as a perfect conductor but for a finite time, the so-called field penetration time. If the RFP configuration eventually will work as reactor, the duration of a discharge will be long enough for any shell to be resistive. To investigate the effects of operating with a resistive shell, EXTRAP-T2 was supplied with a brass shell of field penetration time of 1.5 ms. The duration of a plasma discharge is between 5 and 15 ms and the effect of the resistive shell is shown with the appearance of so-called wall-locked modes [6]. These modes are phase-aligned, stationary field perturbations. At the point where they are locked, particles and energy are lost

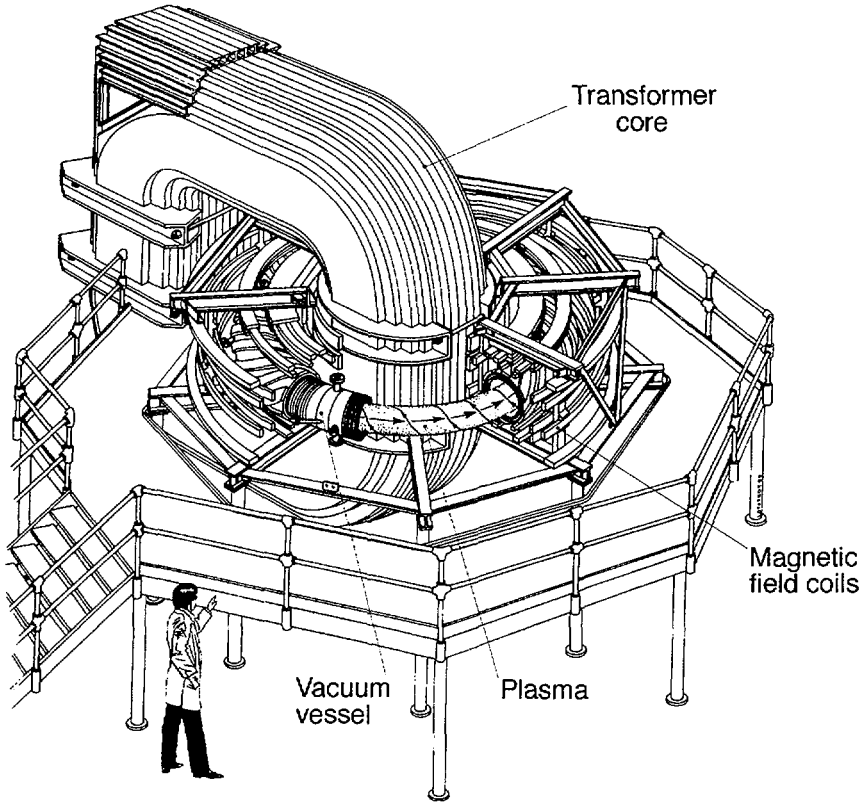

Figure 3.1. A schematic picture of EXTRAP-T2.

to the wall. This leads to local heating of the wall and eventually release of cold particles into the plasma through substantial influxes.

The second important aspect of EXTRAP-T2 is that the vacuum vessel is protected with graphite tiles. The effect of operating with a carbon wall is that it controls the density in a discharge [27]. Approximately 90% of the particles in a discharge comes from recycling with the wall. The density increases steadily in a series of consecutive discharges. Eventually the density gets too high for further operation and the wall has to be cleaned from hydrogen and carbon oxides with helium glow discharge. The lack of control over the electron density makes life a little difficult for the spectroscopists. The electron density is perhaps the most influencing quantity on the radiative emission from the plasma.

Major radius	R	1.24 m
Minor radius	a	0.18 m
Plasma current	I_{p}	$120 - 220$ kA
Loop voltage	V_{loop}	$75 - 125$ V
Average toroidal field	$\langle B_\phi \rangle$	$60 - 150$ mT
Edge poloidal field	$B_\theta(a)$	$120 - 220$ mT
Electron density	n_{e}	$1 - 10 \times 10^{19}$ m^{-3}
Electron temperature	T_{e}	$50 - 200$ eV
Ion temperature	T_{i}	$50 - 300$ eV
Particle confinement time	τ_{p}	$150 - 200$ μs
Energy confinement time	τ_{E}	$20 - 60$ μs
Average ion charge	Z_{eff}	$1.5 - 6.0$

3.2 Spectroscopy at EXTRAP-T2

The port holes of EXTRAP-T2 are small in order to keep disturbing field errors at a minimum. Together with the fact that EXTRAP-T2 has bulky helical field coils makes it difficult to get any wider view of the plasma. Hence, all but two signals are integrated along a single line of sight, usually through the center of the plasma. The only spatial information comes from a three spatial point Thomson scattering system and a five viewing chord visible monochromator.

3.2.1 Active diagnostics

Active diagnostics means that we do something in order to see any light. It can be by injecting a beam of neutral particles or by directing a laser pulse into the plasma. EXTRAP-T2 has no beams but two laser systems.

Thomson scattering. In this system, a short (ns) and intense (J) laser pulse from a ruby laser is fired through the plasma horizontally. The mono-energetic photons are scattered against the electrons. The scattered photons are spread in wavelength, depending on the temperature (velocity) of the electrons and the number of scattered photons depend on the density of electrons. The scattered light is collected from three vertical lines of sight. The recorded signal now comes from a small volume at the intersection of the laser beam and the line of sight. With this setup, the electron temperature

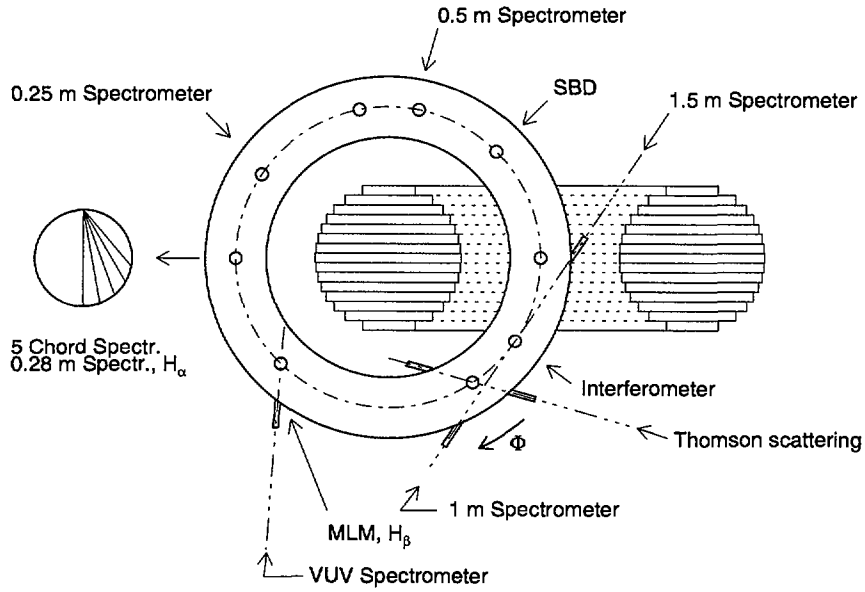

Figure 3.2. An overview of the spectroscopic diagnostics at EXTRAP-T2.

and density are measured at three spatial points at one time in the discharge [28].

Interferometry density measurements. The refractive index of the plasma depends on the electron density. If a laser beam passes through the plasma, the light will be phase shifted. If the phase shift $\Delta\phi$ is measured, e.g. with a Mach-Zender interferometer setup, the line integrated electron density may be calculated from,

$$\Delta\phi = \frac{c'}{\omega}\int n_e dl \tag{3.1}$$

where c' is a constant and ω is the angular frequency of the laser light. The integral is usually divided by the length of the path through the plasma to get the line-average electron density.

3.2.2 Passive diagnostics

A passive diagnostic means that we use the light that is emitted by the plasma. We can not affect the signal (except by how the machine is operated)

and all the data is line integrated. A way to get spatial information of the signal is to view the plasma in different directions.

The passive diagnostics available at EXTRAP-T2 may be divided into three categories, depending on how they select the wavelength of the detected light, and they are spectrometers, monochromators and filters.

Spectrometers. In this instrument the incoming light is dispersed with respect to wavelength with the use of a grating. The dispersed light is imaged onto an extended, multi-channel detector strip, resulting in a wavelength resolved picture of the light. The detector may be an optical multichannel analyzer (OMA) or a charged coupled device (CCD) camera. The wavelength resolution is paid for by low time-resolution, which is on the same order of magnitude as the duration of a plasma discharge.

EXTRAP-T2 has three spectrometers that work in the visible wavelength region. Two of them are high-resolving instruments that are used for ion temperature and velocity measurements. A time-resolution of about 1.5 ms is possible by reading only a part of the OMA detector. The third visible spectrometer has limited wavelength resolution and is used as a survey instrument.

The experiment is also supplied with a vacuum ultraviolet (VUV) grazing incidence spectrometer [29]. Because of the absorption in air of the radiation, the system has to be kept at vacuum. The instrument has three different gratings but the one that has almost exclusively been used during the operation of EXTRAP-T2 is a 450 l/mm grating. With this the wavelength range is 100 Å to 1100 Å. The detector system is a fast OMA (FOMA [30, 31]), which enables one full spectrum every 256 μs. It is a powerful instrument that combines time and wavelength resolution.

Monochromators. A monochromator is essentially the same thing as a spectrometer but it images the dispersed light on a narrow exit slit to get a limited part of the wavelength scale. Since the detector only needs a single channel, very fast detectors such as the photomultiplier (PM) tube is used.

One of the most exciting and inventive diagnostics at EXTRAP-T2 is a five viewing-chord 0.5 m monochromator [32]. Despite the limited view, the lines of sight stretches out from the center towards the edge in steps of 10°, this instrument has supplied the experiment with valuable data on the ion density radial profiles. Together with the Thomson scattering system, this is the only spatial information that is available.

The soft x-ray part of the spectrum can be analyzed with a multi-layer mirror (MLM). This instrument uses a Bragg crystal as dispersing compo-

nent and a microchannel plate or Si(Li) diode as detector. With this system the wavelength range between 20 Å and 60 Å may be studied.

The experiment also has two small monochromators that operate in the visible wavelength region. They are mainly used for monitoring standard spectroscopy signals such as C^{4+} 2274 Å and O^{4+} 2785 Å.

Filters. Instead of using a grating or crystal to select the wavelength of interest in the light, filters can be used for this purpose. In the visible wavelength region, interference filters may be used to select light with very narrow bandwidth, typically 10 Å. These filters consist of several layers of material of different index of refraction. Only the light of the wanted wavelength will interfere constructively and pass through the filter while all other wavelengths will interfere destructively and be reflected. A filter can in this way be used as a mirror, where a specific part of the spectrum is transmitted and the rest reflected to be used at some other point in the detection system. Using filters instead of monochromators means loss of flexibility but the system is much cheaper and more important, several orders of magnitude more sensitive. The sensitivity is particularly important when it comes to detecting weak continuum radiation.

Filters in the visible are used to measure hydrogen line emission, e.g. H_α, or continuum radiation. The detector is normally a PM-tube. Radiation in the x-ray wavelength region, which otherwise can be difficult to observe, can be detected with a system consisting of a thin metal film that prevents radiation below a certain energy range to pass through. The detector here is a surface barrier diode (SBD).

3.3 JET

One part of the work presented in this thesis, paper VII, was performed at the JET[1] Joint Undertaking, which is the worlds largest fusion experiment. It is based on the tokamak concept and it is a collaboration between the 14 countries in EURATOM.

The poloidal cross-section of JET is not circular as in EXTRAP-T2 but more like almond-shaped. The height of the vacuum vessel is 3.96 m and the width is 2.4 m. The torus radius (or major radius) is 3.1 m. JET can be operated with up to 5 MA of plasma current and with a toroidal magnetic field of up to 4 T.

JET has shown reactor relevant conditions for ion temperature, ion den-

[1] Joint European Torus.

sity and energy confinement time. The experiment holds the world record on fusion power and fusion energy produced [33, 34]. In the record discharges, the fuel was a $50 - 50\%$ mix of deuterium and tritium. These studies are very important since they are close to the situation that will be in a future fusion reactor. D-T studies have previously been performed at TFTR[2] [35]. However, these D-T discharges produce a number of neutrons from the fusion reaction. These high-energy neutrons activate the wall material. To avoid this, JET is fueled with 100% deuterium except in dedicated D-T experiments.

Being such a big experiment, JET is of course very well-diagnosed. However, only the instrument used in paper VII will be described here.

This instrument is a bent crystal spectrometer with a very long focal length, 25 m [36]. This gives a high wavelength resolution of $\lambda/\delta\lambda \sim 20000$. The ion temperature in the center of the plasma is routinely monitored with this instrument and the $1s^2\ ^1S_0 - 1s2p\ ^1P_1$ transition in Ni^{26+} is used for this purpose. The dispersing element is Ge(220) crystal and the detector is a multi-wire proportional chamber (MWPC).

The line of sight of the instrument depends on the wavelength and was originally through the center of the plasma. In connection with a rebuild of the divertor in JET, the inboard wall was supplied with new guard limiters. This effectively moved the line of sight closer to the inboard wall and for some wavelengths they now intersect. This has led to a decrease in the free spectral range of the instrument. It also means that more of the signal from the plasma edge is now recorded. Contributions of charge exchange excitation from fully stripped chlorine and background neutral deuterium have been observed in chlorine line emission as a consequence of this. This is reported and investigated in detail in paper VII.

[2]The Tokamak Fusion Test Reactor at Princeton, New Jersey, USA.

Chapter 4

Impurities

One of the most essential parameter to know in a fusion experiment is the average ion charge, Z_{eff}. In the end of the first chapter it was made clear that this parameter must be kept at a minimum or radiation losses will prevent the dream of nuclear fusion power production to come true. Even at perhaps more modest circumstances, when one does not try to achieve fusion but to advance in understanding the plasma and improving the operation of an experiment, Z_{eff} is an important number. It is a measure of how clean the plasma is, and the more dirty it is the more resistive it gets with higher losses as a result. In the last part of this chapter is a brief summary of the observations on resistive shell operation and in particular the effect on impurity content and Z_{eff}.

There are three different ways of determining the average ion charge. The first is based on bremsstrahlung radiation, usually measured in the visible wavelength region. The second is by calculating the density of impurity ions and sum their contribution to Z_{eff} and the third is from the resistivity of the plasma, calculated from toroidal current and voltage.

4.1 Impurity measurements from visible bremsstrahlung

The most commonly used method to determine Z_{eff} is the one based on continuum radiation or bremsstrahlung [37]. This kind of radiation comes from the fact that when charged particles are forced to accelerate or decelerate they will emit radiation. Such an event is when the trajectory of a free electron is bent because of the attractive Coulomb interaction with an ion. The intensity of the emitted bremsstrahlung $\varepsilon_{\text{brem}}$ for a given wavelength λ (Å)

depends on the electron temperature T_e (eV), electron density n_e (cm^{-3}), the ion density n_i (cm^{-3}) and the ion charge Z_i,

$$\varepsilon_{brem} = \frac{1.5 \times 10^{-29} n_e n_i Z_i^2 \bar{g}_{ff} e^{-\frac{hc}{\lambda T_e}}}{\lambda^2 \sqrt{T_e}} \quad [\text{W cm}^{-3}\ \text{sr}^{-1}\ \text{Å}^{-1}] \tag{4.1}$$

where $\bar{g}_{ff}$ is the free-free Gaunt factor [38], that essentially is the difference between a classical and a quantum mechanical treatment of the bremsstrahlung and may be approximated by [39],

$$\bar{g}_{ff} = 3.77 \frac{(0.001 T_e)^{0.147}}{(Z_{eff})^{0.0579}} \tag{4.2}$$

When the contributions from all the ions are summed, the bremsstrahlung is given by,

$$\varepsilon_{brem} = \frac{1.5 \times 10^{-29} n_e^2 \bar{g}_{ff} e^{-\frac{hc}{\lambda T_e}}}{\lambda^2 \sqrt{T_e}} \frac{\sum n_i Z_i^2}{\sum n_i Z_i} \quad [\text{W cm}^{-3}\ \text{sr}^{-1}\ \text{Å}^{-1}] \tag{4.3}$$

The last term, the ratio between the two sums is the definition of Z_{eff}. Thus, if we measure the bremsstrahlung in the visible wavelength region and calibrate the signal in absolute numbers, we have a simple formula for directly calculating Z_{eff} if we only know the electron temperature and density.

This technique is a standard diagnostic at most fusion experiments but there are two things one has to be careful with when recording continuum radiation for this purpose.

The first thing is to assure that there are no spectral lines that are contaminating the measurement. Visible bremsstrahlung is a weak signal but even spectral lines that are considered to be insignificantly small in comparison with more prominent spectral lines, may still be an order of magnitude more intense than the bremsstrahlung. As almost all bremsstrahlung measurements are performed with a system of interference filters and PM-tubes that lack the wavelength resolution, it is very important that the spectral region of interest has been studied with spectrometers before any quantitative work take place. Since the dependence on electron density is stronger for the bremsstrahlung than for spectral line emission (equation 2.7) the problem of contaminating line emission is greater at low electron densities. It is possible that the very high values for Z_{eff} that is quoted in fusion experiments

at low electron densities is the result of contaminating weak spectral lines. This problem is likely to vanish when operating at higher electron density at which the bremsstrahlung radiation gets stronger. However, when recording bremsstrahlung with a detection system without spectral resolution, the risk of the presence of however weak spectral lines is a constant source of concern.

The second thing that one should know about, even though it most of the time will not mean any problem, is radiative recombination. This is the process when a free electron recombines with an ion and enters a bound state. The excess in energy, the kinetic energy of the electron and the binding energy of the bound state, is released in the form of a photon. Since the free electrons have a continuous range of kinetic energy, so will the emitted radiation display a continuous spectrum of wavelengths. Recombination radiation may be expressed in similar form as the bremsstrahlung (equation 4.1) [40, 41],

$$\varepsilon_{\mathrm{rec}} = 2\frac{1.5 \times 10^{-29} R_{\mathrm{y}} n_{\mathrm{e}} n_{\mathrm{i}} Z_{\mathrm{i}}^4 e^{-\frac{hc}{\lambda T_{\mathrm{e}}}}}{\lambda^2 T_{\mathrm{e}}^{3/2}} \sum_{n=n^*}^{\infty} \frac{\bar{\mathrm{g}}_{\mathrm{bfn}}}{n^3} e^{\frac{Z_{\mathrm{i}}^2 R_{\mathrm{y}}}{n^2 T_{\mathrm{e}}}} \tag{4.4}$$

where R_{y} is the Rydberg energy, or the ionization energy for hydrogen, 13.6 eV and where $\bar{\mathrm{g}}_{\mathrm{bfn}}$ is the bound-free Gaunt factor. The dependence on electron temperature and ion charge is different than for the bremsstrahlung. The different ion dependence prevents us from writing equation 4.4 on the same form as the bremsstrahlung, with Z_{eff}. The last term, the sum, deals with which n-shell the electron may enter. If we use the simple Bohr model for the atomic levels, the principal quantum number n of the lowest energy level of an ion of charge Z_{i} that an electron may enter with the subsequent emission of a photon of wavelength λ, is given by,

$$\frac{R_{\mathrm{y}} Z_{\mathrm{i}}^2}{(n^*)^2} \leq \frac{hc}{\lambda} \tag{4.5}$$

In order for the recombination radiation to be comparable to the bremsstrahlung, n^* has to be equal to one and the exponent in the sum must be large. In other words, the photon energy must be much larger than the electron temperature for recombination radiation to dominate. This means that in the visible wavelength range where the photon energy is on the order of 1 eV, which is much less than the electron temperature, continuum radiation will be only bremsstrahlung. At the plasma edge where the electron tem-

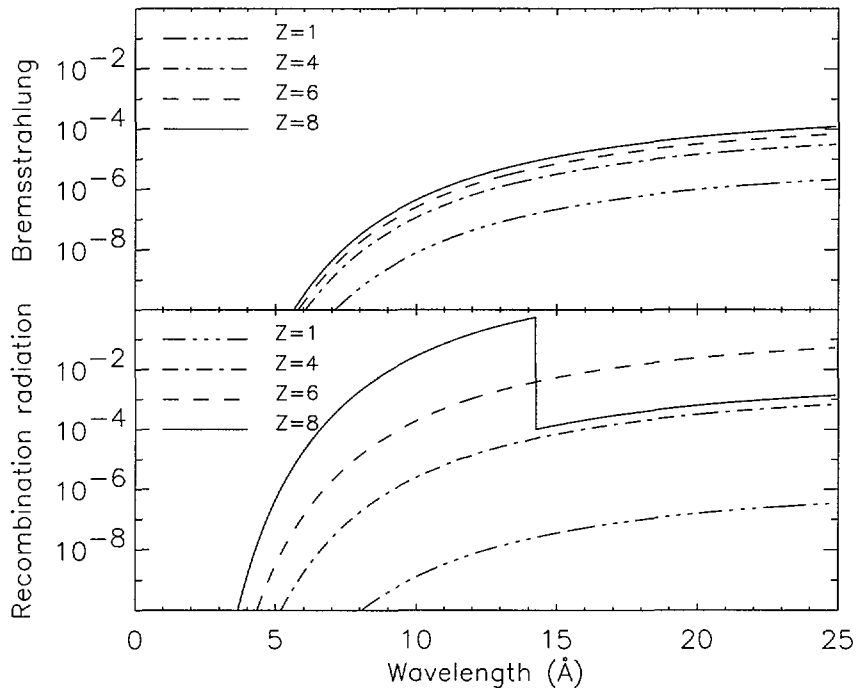

Figure 4.1. Bremsstrahlung (top) and recombination radiation (below) for Z=1, 4, 6 and 8. To get the actual emitted radiation, the plotted curves must be multiplied with the abundance of each ion. Therefore Z=8 will not be the dominating charge because of its low density. Recombination will be dominated by Z=6 and bremsstrahlung by Z=1 and 4. The sharp increase in the emission from Z=8 at 14 Å is because the n=1 shell becomes available for recombination at this energy (equation 4.5).

perature is of the order of the photon energy the recombination radiation will still only be about a few percent of the bremsstrahlung.

In the soft x-ray wavelength region where the photon energy is indeed larger than the electron temperature (EXTRAP-T2 condition) recombination radiation will dominate. The bremsstrahlung and recombination radiation is shown in figure 4.1 in the wavelength range of interest for the surface barrier diodes. The intensity in the emission from each ion must be multiplied with the abundance of that ion to see how much each will contribute.

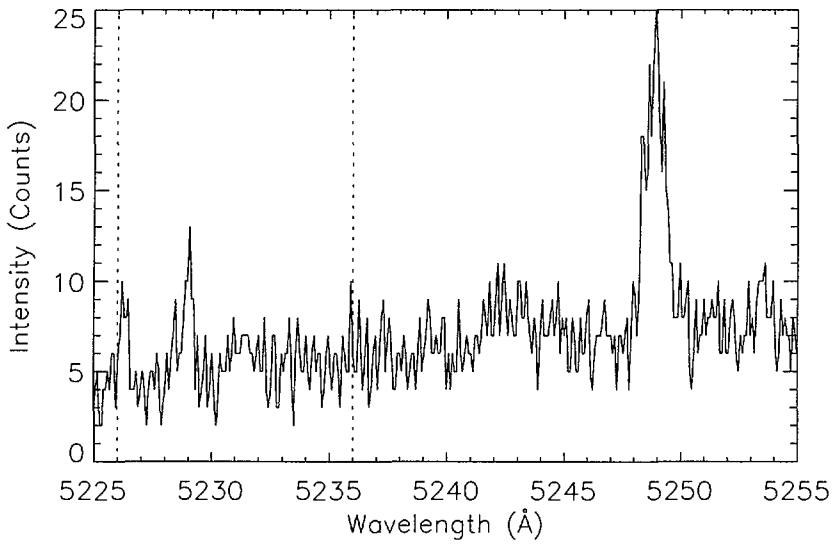

Figure 4.2. Spectrum around 5230 Å. The vertical dotted lines indicates the transmission window of the interference filters that are used for the visible bremsstrahlung measurement. There are clearly two spectral lines within the filter window and it is possible that a great part of the background is made up of weak spectral lines. This effectively prevents the calculation of Z_{eff} from these measurements.

In total the bremsstrahlung is only about 1.5% of the continuum radiation. The bremsstrahlung is made of 50% from Z=1 and 30% from Z=4. The recombination radiation owes more than 75% of its intensity to Z=6, mainly from the O^{6+} ion.

4.1.1 Measurements at EXTRAP-T2

Visible bremsstrahlung has been measured in EXTRAP-T2 with the purpose of calculating Z_{eff}. Except when the electron density is high, on the level of 5×10^{19} m^{-3}, the calculated value of Z_{eff} is too high. The reason for this is that the signal recorded is not only bremsstrahlung but also contains signal of another kind. The system used for the measurement consists of two identical interference filters and a PM-tube. The filters transmit light at 5230 Å and with a bandwidth of 10 Å. Two filters, rather than one,

were used to get a strong depression of signal outside the wavelength range of interest. The ratio between transmission within the bandwidth of the filters and outside of it is about 10^9 so the effect of spectral lines outside the filter window is negligible. The effect of recombination radiation can be ruled out since the photon energy is about 2.4 eV and with support from the discussion in the previous section. Left is only the effect of spectral line emission within the filter bandwidth.

A spectrum over the wavelength range of the bremsstrahlung measurement is shown in figure 4.2. There is clearly a spectral line at 5229 Å, i.e. within the filter window. A careful look may also give that there seems to be a number of weak lines making most of the background level. The electron density in this case is 5.0×10^{19} m^{-3}. If we assume an electron temperature of 75 eV (see electron temperature scaling in paper I, figure 5), the bremsstrahlung measurement (PM+filters) gives Z_{eff} of 3.6. If we subtract the signal above the lowest level in the spectrum we end up with Z_{eff} of 1.8, which is consistent with the VUV measurement (again paper I). If the density is lower, around 2.0×10^{19} m^{-3}, Z_{eff} is around 15-20. The spectral lines seen in figure 4.2 are there but the signal is too low to say where the lowest level is, and it is difficult to repeat the calculation. Now this is of course not the way to perform a measurement anyway but it might help in understanding the problem with the visible bremsstrahlung measurement.

4.2 Impurity content from VUV line emission

The way to measure ion densities were described in chapter 2. If we measure the intensity of a spectral line, we can calculate the ion density from,

$$I = n_z n_e q_{ij} \frac{A_{ij}}{\sum A_{ij}} \tag{4.6}$$

If we do this for every ionization stage of every species present in the plasma, we may sum their contributions to Z_{eff},

$$Z_{\text{eff}} = \frac{\sum n_i Z_i^2}{\sum n_i Z_i} \tag{4.7}$$

This way of calculating Z_{eff} is more complicated than using visible bremsstrahlung, and admittingly exposed to more sources of error but there are also rewards. It gives a better understanding of the plasma as we not only know how clean/dirty the plasma is but also what impurity species there

are and in what quantities. The analysis also contains estimation of the particle confinement time, τ_p and the electron temperature, both important to know.

An ion emits line radiation in a broad range of wavelengths. Since the calculations (equation 4.6) are only based on one or two spectral lines for a given ionization stage, we only sample a part of the emitted radiation. It is therefore important that we select intensive spectral lines to ensure that the measurement includes as much as possible of the radiation. This can be done by measuring so-called resonant spectral lines, transitions that end in the ground state[1]. All the ionization stages up to lithium like carbon (C^{3+}) and oxygen (O^{5+}) have resonant transitions in the part of the wavelength region that is covered by the VUV spectrometer. In one spectrum, all the necessary information is recorded.

The ion densities for the higher ionization stages may of course also be calculated from measured spectral line emission. One problem, if resonant transitions are to be used, is that they are in the soft x-ray or even x-ray wavelength region and that absolute calibration is difficult at these short wavelengths. A solution to this could be to use non-resonant transitions that are in a more easy-calibrated wavelength region but with the problem of estimating the ion density from a small part of the emitted radiation. Another way is to calculate the density of the higher ionization stages from the lower ones in an ionization balance (equation 2.11)

$$\frac{n_z}{\tau_p} = n_{z-1} n_e S_{z-1,z} \tag{4.8}$$

This has been done for helium-like carbon and oxygen, C^{4+} and O^{5+}. In order to perform this calculation τ_p has to be determined.

The particle confinement time, τ_p, is given by,

$$\tau_p = \frac{\int n_p dV}{\int \Gamma_H dA} \tag{4.9}$$

The plasma is assumed to be quasi-neutral, i.e. if we look in a volume that is sufficiently big, the number of positive charges equals the number of negative charges. With this the proton density, n_p, can be calculated with,

[1]This expression can be a little confusing. A process is resonant when the available energy perfectly match the required energy. A transition between two bound states with the emission of a photon is a resonant process, no matter if the final state is the ground state or not.

$$n_{\mathrm{p}} = n_{\mathrm{e}} - \sum_{i \neq p} n_{\mathrm{i}} Z_{\mathrm{i}} \tag{4.10}$$

Since we need the particle confinement time for calculating the density of the higher ionization stages, and these densities are needed in equation 4.10, the whole calculation must be performed self-consistently.

The influx of hydrogen atoms, Γ_{H}, is more difficult to calculate. It can be done using the ionization per photon concept described in chapter 2 but this is a zero-dimensional calculation. The balance between the influx of neutral hydrogen and the ionization occur at the edge of the plasma. To take this into account and not use a model where the line-average electron density and temperature comes in, a different approach is possible where the radial profiles for temperature and density are included. In this model, the neutrals enter the plasma with a fixed velocity v_{o} and get ionized on their way towards the center. The influx is now given by the velocity times the neutral density at any point and the neutral hydrogen density, at steady-state is given by [42],

$$\Gamma_{\mathrm{o}}(r) = v_{\mathrm{o}} n_{\mathrm{o}}(r) \tag{4.11}$$

$$\frac{1}{r}\frac{\partial}{\partial r}(r\Gamma_{\mathrm{o}}(r)) = -n_{\mathrm{o}}(r) n_{\mathrm{e}}(r) S_{\mathrm{o}}(r) \tag{4.12}$$

where the radial dependence on the ionization rate S_{o} comes from the dependence on electron temperature and density and their radial dependence. Equation 4.12 can be solved, giving the density of neutrals with respect to radius, $n_{\mathrm{o}}(r)$. When the neutral density is known, the intensity of any transition may be calculated. This is usually done for H_α and the calculated intensity, at unit influx, is integrated with respect to radius along the same path as the measurement of the transition. The influx of neutral hydrogen is now determined by comparing the measured intensity with the calculated intensity at unit influx.

One problem with the calculation of Γ_{H} is that it is difficult to measure the H_α radiation as a global parameter. The particle confinement time is assumed to be valid for all the plasma and so are the densities and temperatures that are included in the calculations. But we are depending on the measurement of a very local signal, H_α. There is not enough coverage of the emission from EXTRAP-T2 plasmas to say that we have a clear picture of the hydrogen emission. Instead it is limited to a few places, with single

lines of sight. At the time of the frequent influx event in EXTRAP-T2, the electron density increases perhaps a factor of two or three. This leads to that the proton density in equation 4.10 will increase. If our local measurement is off the place for this event, there will be no increase in the H_α emission and therefore no increase in Γ_H. With this we will obtain a higher value for the particle confinement time even though it has not increased at all. To solve this problem, at least somewhat, τ_p was calculated from a series of discharges where there were no influx events and the electron density and the H_α emission were constant. In this series, τ_p was between 150 and 200 μs. This range of values has been used in all calculations involving the particle confinement time.

In the calculation of Z_{eff}, only carbon and oxygen was included and no ionization stage above helium-like. Is it possible to disregard other species and higher ionization stages? To start with, in all the spectra recorded there has been no metals and only traces of nitrogen. It is therefore safe to say that other impurities than carbon and oxygen have no effect on the impurity content of the plasma. The second question is if there are no hydrogen-like or even fully stripped carbon or oxygen. The answer is that these ions exist but in so small amounts that they do not change the overall view of the impurity content.

The electron temperature in EXTRAP-T2 is around 100 eV. The energy required to open up the $1s^2$ level is 392 eV for carbon and 739 eV for oxygen. This means that it will take long time to produce H-like ions. The characteristic time $1/(n_e S)$ for ionization here is 10 ms (C) and 1 s (O) at an electron density of 2.0×10^{19} m^{-3}. With a particle confinement time of 200 μs, the density of H-like carbon will be 0.02 of the He-like carbon and subsequently less for oxygen. The density of C^{4+} is typically around 1.0×10^{18} m^{-3}. With this the contribution to Z_{eff} is 0.6 for C^{4+} and 0.02 for C^{5+}. This means that as far as contribution to the impurity content and Z_{eff} is concerned, higher ionization stages than He-like may be neglected. However, these small densities can still be of importance for studies of spectral line emission.

4.3 Plasma resistivity and anomalous power

The third way obtaining Z_{eff} is from the plasma resistance. It has been mentioned that the dirtier (higher Z_{eff}) the plasma is the more resistive it

is. The resistivity is also dependent on the electron temperature, a cold plasma is more resistive than a hotter.

The resistivity parallel to the magnetic field is given by [43],

$$\eta_{\|}(r) = \frac{3.04 \times 10^{-5} \ln \Lambda Z_{\text{eff}}(r)}{\gamma T_{\text{e}}(r)^{3/2}} \tag{4.13}$$

where γ is a function of Z_{eff} and $\ln \Lambda$ is the so-called Coulomb logarithm and has a value around 15 for fusion relevant plasmas. We can now calculate the so-called Spitzer power P_{s} by integrating the resistivity times the square of the current density over the the plasma volume (assuming $j_{\perp} \ll j_{\|}$),

$$P_s = \int\int\int \eta_{\|}(r)(j_\theta(r)^2 + j_\phi(r)^2) dV \tag{4.14}$$

The poloidal and toroidal current densities can be calculated with the PFM-model (see figure 1.4). The radial dependence on the resistivity comes from the electron temperature and Z_{eff}. Thomson scattering measurements show that the electron temperature profile has a form of $T_{\text{e0}}(0.9(1.0 - (r/a)^4) + 0.1)$. To measure Z_{eff} in RFP's are difficult, and to the best of my knowledge there has been no report on the spatial dependence on Z_{eff}. One way to estimate the profile is to use a one-dimensional ionization balance including transport [42]. The radial dependence of carbon and oxygen ions has been investigated with the five viewing-chord monochromator and the result has been compared with the transport calculations [44]. We now get the radial profiles for all the ions of interest and the absolute level of the ion densities from VUV measurements. By summing the contributions from the different ions we get $Z_{\text{eff}}(r)$. The result of this calculation is shown in figure 4.3 which also shows the radial profile of $\eta_{\|}$, with and without $Z_{\text{eff}}(r)$. Electron temperature is clearly the dominating term and Z_{eff} can be taken outside the integral.

The Spitzer power has been calculated from a set of discharges (the same that is used in paper I) and been compared to the input power, P_{in}, which may be divided into two parts, the Spitzer power and the so-called anomalous (or non-Spitzer) power, P_{a},

$$P_{\text{in}} = P_{\text{s}} + P_{\text{a}} \tag{4.15}$$

The anomalous power is thought of being the part that is put into the dynamo to keep it going and may be a measure of the efficiency of the dynamo [45]. It is also the anomalous power that is believed to be the

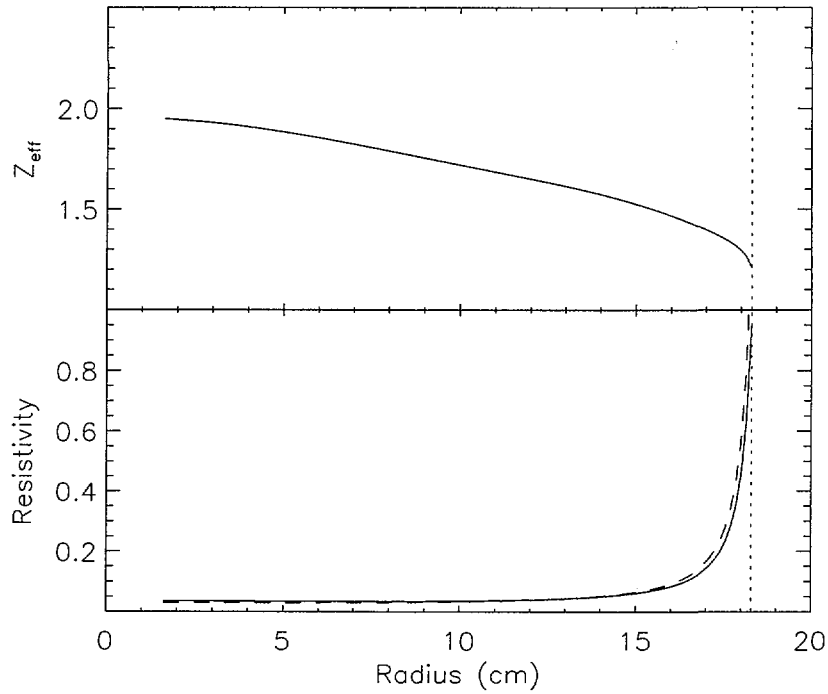

Figure 4.3. Top: The radial profile of Z_{eff}. Below: The normalized parallel resistivity profile $\eta_{\|}$ with the radial dependence on Z_{eff} included (full line) and without (broken line). The line-average value of Z_{eff} was used in the later case.

source of extra heating of the ions as the ion temperature is measured to be higher than the electron temperature in RFP's.

If $\eta_{\|}$ is assumed to be uniform there appears indeed to be an anomalous part in the power balance, but the inclusion of the radial dependence in $\eta_{\|}$ makes this less obvious. On the average there might be an anomalous part of less than 10% of the input power but there is a great deal of scatter in the data. The discrepancy between P_{in} and P_{s} can also be removed by a modest change in the electron temperature profile. If there is such a thing as anomalous power, it is, as far as this calculation goes, hidden within the inaccuracy of the radial profile measurements.

4.4 Resistive shell operation and impurity content

The main objective for EXTRAP-T2 is to study the effects of operating a reversed-field pinch with a resistive shell. The result is a toroidally localized, wall-locked mode that significantly degrades the confinement. The localized perturbation results in enhanced plasma-wall interaction and strong influxes of hydrogen and impurities, mainly carbon but also oxygen.

The wall-locked mode is present in every discharge and from the very beginning of it. It shows itself with a strong radial magnetic field, $B_r/B \sim 5\%$. The magnetic field is disturbed, the field lines intersect the wall at the point of the locking, feeding energy and particles to the wall. In connection to the mode is also the generation of toroidal flux by the dynamo at the position of the locking.

At the point where the mode is locked, the loss of energy and particles leads to a local heating of the wall. This in turn leads to influx of hydrogen and impurities to the plasma. The burst of released particles is correlated in time with the bursts of toroidal flux. There is however no strict relation between the amplitude of the mode (B_r) and the influx of particles. The amplitude of the influx instead has a strong dependence on the plasma current.

There are in principle three operational regimes in EXTRAP-T2, and they are related to the plasma current. When the current is 150 kA, the influxes are small and does not disturb the plasma globally. At 175 kA there is almost always a strong influx around 4 ms into the discharge with the result that the electron density goes up with more than 50% and the plasma current drops. The electron temperature decreases, the impurity content increases, mostly from carbon. Z_{eff} goes up and the plasma gets more resistive. After the influx event the plasma recovers somewhat, the electron density as well as impurity content decreases. Z_{eff} goes down and the plasma enters a clean but cold and resistive state. The discharge may last for almost 10 ms after this and usually ends in slow but steady increase in carbon content. When the plasma is operated at 200 kA of plasma current, these influx events are usually so strong that the discharge terminates.

Chapter 5

Summary of papers

In this chapter a brief summary of each paper will be given. In the papers where I appear as a co-author I have supplied with spectroscopic measurements of mainly electron temperature and impurity ion densities (and some quantities derived from them) and also participated in the discussion of the paper. I have written the paper where I stand as first author, except for paper VII where the manuscript was co-written with Klaus-Dieter Zastrow.

5.1 Paper I

The main purpose of the study in Paper I was to obtain the electron temperature and the average ion charge Z_{eff} and to study their temporal behaviour in the three operational regimes, 150, 175 and 200 kA of plasma current. The measurement was performed with an absolutely calibrated VUV spectrometer and the calculations were based on spectral line emission and a collisional-radiative model.

The ion densities of lithium-like carbon and oxygen were calculated from resonant transitions using an excitation balance. The helium-like ion densities were calculated with an ionization balance. The electron temperature that was needed to determine the value for the various rate coefficients was calculated from two line ratios in O^{5+}. In the ionization balance, steady-state was assumed and the increase in helium-like ions are balanced by the loss of particles with the time-scale of the particle confinement time. This quantity was calculated from the influx of hydrogen atoms which was estimated from measurements of hydrogen line emission.

The main result was the establishment of the values for the electron tem-

perature, impurity ion densities, particle confinement time and Z_{eff}. The study showed that the strong influx event that is almost always present in 175 kA discharges and that terminates the higher current discharges leads to a strong increase in carbon content, in some cases as much as a fourfold increase. It was also seen that in the aftermath of the influx event, if the discharge survives, the plasma is characterized to be cleaner but colder and more resistive. The ratio between the carbon and oxygen content was established, about 4:1, more or less independent with respect to I/N. It was also noted that despite the fact that the graphite wall make carbon the most abundant impurity species, oxygen makes a significant contribution to Z_{eff} due to its higher charge.

One important conclusion concerns the I/N dependence on Z_{eff}. There is a clear, although not drastic increase in Z_{eff} as I/N goes up, mainly due to a decrease in electron density. Now, this is not too surprising but the interesting thing is that, even at very high values of I/N, Z_{eff} is limited to a value around 4. Compared to Z_{eff} measurements from visible bremsstrahlung with the electron density at the low limit, these measurements usually show a high (and sometimes too high) value for Z_{eff}. The conclusion is that visible bremsstrahlung measurements are limited to high electron densities where the effect of contaminating line emission is minimum.

5.2 Paper II

The purpose of this paper was to report on charge exchange contribution to the emission of the 5290 Å transition in C^{5+} and how this can be used to estimate the density profile of neutral hydrogen. But one could also say that the paper shows that the simple tomographic system employed by Jesper Sallander can be used for quantitative work (the first paper on this instrument [32] only contains emission distribution with respect to impact parameter and therefore represents a more qualitative view of the spatial distribution) and that this is exemplified by the study on charge exchange excitation of C^{5+}. This view of the paper is closer of how it came to be and it is also an interesting story of how rewarding it can be if one is prepared to spend quite a substantial amount of time to explain something that is not understood at all from the beginning.

When we first started doing measurements with the five viewing-chord system we were anticipating interesting results and confident that it would work. This optimism was based on simulations that showed that, as long as

the emission was peaked, it would be possible to reconstruct the emission radial profile accurately. We started with C^{4+} emission, C^{4+} being assumed to be the most abundant ion and having a peaked profile, but the result was far from satisfactory. Since the simulations showed that the more peaked the emission profile was, the easier it would be to do the reconstruction. The decision was made to look at C^{5+} emission and the choice fell on the n=8-7 transition at 5290 Å.

But C^{5+} gave no evidence that we were on the right track, quite the opposite. Here we had an ion that must have a peaked ion density profile and yet we saw a lot of signal from the edge. Even more strange, in some discharges the emission was even peaked towards the edge and the emission profile could even change during a discharge.

With a little less time and patience available, the conclusion that a system of only five lines of sight was insufficient for quantitative studies, would have been close at hand. But curiosity and the desire to explain the strange data helped and the complex emission profile from C^{5+} not only helped in realizing that the five viewing-chord system could be very useful, it also provided the key to how to analyse the data.

At some point it was suggested that the emission from the edge was caused by excitation by charge exchange collisions between neutral hydrogen and fully stripped carbon. To test this hypothesis, the emission was calculated with one-dimensional excitation balance with one part being electron collision excitation for C^{5+} and one part charge exchange collision excitation with neutral hydrogen and C^{6+}. The ion density profiles were taken from a one-dimensional ionization balance (including transport) and the electron density and temperature profiles from Thomson scattering. The absolute level of the carbon content was based on VUV measurements. The emission was then integrated along the different lines of sight for the instrument and the integrated signal was compared with the measured one. The free parameter in the fit was the neutral hydrogen density, the absolute level as well as the profile.

It worked and it showed that the emission indeed contains two parts, electron collision excitation and charge exchange excitation. With this it was possible to estimate the neutral hydrogen density profile and also to study the effect of a minor influx event (no global effect). It also showed the way of how to treat the limited spatial information from only five lines of sight. Rather than inverting the emission profile and from there calculating the ion density profile, the solution is to describe the ion density with a set

of functions (later Zernicke polynomial), calculate the emission with a one-dimensional excitation balance, integrate the emission with respect to the lines of sight and finally fit the ion density profile to the measured signal.

It is my personal belief that this is the true merit of the paper, to show how such a simple system can be used and how to analyze the data from it. This technique was used in later work (among them paper VI).

My contribution to the paper was to supply the data on the carbon concentration and the particle confinement time that was used in the transport calculations together with many hours of discussions before the problem was solved.

One point of clarification concerns the comparison between the transport calculations and the VUV measurements (table 1 in paper II). In the VUV measurement the electron temperature was 80 eV and the electron density 2.0×10^{19} m^{-3} compared to 150 eV and 4.0×10^{19} m^{-3} in the transport calculation. This changes the relative abundances of the different ionization stages, although the temperature and density in the transport calculation is the value on axis. The particle confinement time is also different, 175 μs and 200 μs.

In the attempt to explain the absolute level of the emission, both the density of C^{5+} and C^{6+} needed to be high, as well as the electron temperature. Since $T_e \ll E_{exc}$ (482 eV), the rate coefficient for electron excitation is strongly dependent on T_e. The values used in the calculation on the absolute scale was taken to be the maximum of the accepted parameter range and are probably too high. Despite this, there is still a factor of 20 and of 25 too much light recorded in the electron excitation part and in the charge exchange part, respectively.

Why do we see to much light? Several possibilities for these discrepancies have been investigated.

The rate coefficient for electron collision excitation in C^{5+} is valid for collisions with ions in the ground-state. If the excitation would involve ions in the metastable state 2s, the excitation energy decreases from 482 eV to 115 eV. This is close to the electron temperature and so the rate coefficient is much higher. However, the increase in rate coefficient is not sufficient because of the low density of the 2s state and it is concluded that the metastable level has no effect.

The H 2s metastable state is important for the charge exchange collision excitation. The calculation of the density of the 2s state was based on the assumption that excited states in hydrogen are created by electron collisions

with hydrogen atoms in the ground state. The true picture is probably more complicated than that. Molecular hydrogen enters the plasma from the wall and may be excited, ionized or dissociated by electron collisions. Some of the excited states are not stable and the molecule dissociates. The fragments are likely to be in excited states. This can lead to a different density of the 2s state and will therefore affect the charge exchange part of the emission.

Another possible explanation is that it is difficult to calculate the ion density when only a very small fraction of the light emitted by the ions are collected and the 5290 Å transition is weak with respect to other C^{5+} spectral lines. But one would expect that the effect of this would be a scattered result in ion density, not a systematic deviation.

There are uncertainties in the rate coefficients and the density of hydrogen in metastable states that might offer the solution. But there might also be a hint in the fact that both the emission from electron collision and charge exchange exceed the expected intensity by approximately the same amount.

5.3 Paper III

The aim of this paper was to summarize the experiences and observations of operating a reversed field pinch with a resistive shell and a graphite wall.

Magnetic field measurements show the presence of a toroidally-localized, wall-locked mode. Associated with the mode is a $\sim$ 10% increase in the toroidal flux at the position of the locking, and a large radial magnetic field, $B_r/B \sim 5\%$. The degradation of the magnetic field topology is confirmed in a resistive MHD calculation. The distortion of the magnetic flux surfaces leads to an enhanced plasma-wall interaction, with the loss of particles and energy, at the position of the locking. Local heating and release of hydrogen, carbon and oxygen follows.

Pictures from a camera, equipped with an infrared filter, show the existence of local, bright spots with temperatures exceeding 1000 K and covering about 2% of the wall. A hydrogen recycling model can simulate the density increase by assuming the wall temperature and the extent of the hot spots, measured with the camera.

Measurements of VUV line emission show that the increase in electron density is accompanied by a strong increase in mainly carbon but also oxygen content and a drop in electron temperature. The influx somewhat heals the wound of the wall-locked mode and allows the plasma discharge to continue

long after the influx. The plasma now enters a cleaner but colder and more resistive state.

If the wall-locked mode activity could be reduced to the level of other magnetic fluctuations present, model calculations suggest that there would be a more than 50% increase in electron temperature at the same time as a the loop voltage decrease with 50%. The net effect would be an increase in energy confinement time by a factor of three.

One conclusion is that the wall-locked mode is present from the beginning of every discharge. This means that it is present before a good RFP equilibrium is set up. The thought is that if the shell time is longer than the time it takes to reach maximum current, the wall-locked mode, that grows on the time-scale of the shell time, will not be present during the sensitive start-up phase and that the RFP configuration will be able to withstand it better later on.

5.4 Paper IV

The graphite wall in EXTRAP-T2 controls the density. About 10% of the particles comes from the gas puff before the discharge and the rest comes from the wall. With every discharge, the amount of hydrogen trapped in the graphite increases and this leads to a steady increase in the plasma density in a series of consecutive discharges. A number of models have been tested to predict and understand the hydrogen recycling and this is reported in paper IV.

To explain the density behaviour in a discharge, the density increase in a series of discharges and the hydrogen removal by helium glow-discharge cleaning, zero-dimensional models were sufficient. In order to explain the effect of an isotope exchange experiment, where the initial gas puff is with deuterium instead of hydrogen, a one-dimensional model that includes diffusion, trapping and de-trapping of atoms and molecules in the graphite was employed. The change in hydrogen and deuterium concentration was monitored by recording the H_α and D_α emission with a high-resolution spectrometer. The ratio of the intensities equals the ratio of hydrogen and deuterium densities. The measured ratio was compared with the result from the model calculations, both the temporal behaviour within a discharge as well as in a series of discharges. The result shows that diffusion in the graphite must be included for the model to be able to reproduce the measured density ratio. The experiment was then reversed, hydrogen was once again used in the

initial gas puff. The model now reproduces without problem the decrease in deuterium concentration.

My contribution to the work are the spectroscopic measurements and analysis of the data, supplying David Larsson with the density ratios. In terms of spectroscopy, it is simple work but it shows that even simple measurements can give valuable results.

5.5 Paper V

The radiation with energies above 500 eV (24 Å) is routinely monitored with two surface barrier diodes (SBD). In some discharges, the soft x-ray emission displays large amplitude oscillations ($\sim$ 10%) with frequencies around 15 kHz. These oscillations are seen on both SBD's, which are separated by 180°. At the same time, at one toroidal position, the poloidal loop voltage shows similar fluctuations, but anti-correlated in time. The fluctuation in the poloidal loop voltage, or the toroidal flux, is toroidally localized dynamo activity. This non-symmetric production of toroidal flux has been linked to the wall-locked mode.

At the same toroidal position as the poloidal loop voltage measurement, line emission, e.g. H_α show the same pattern, anti-correlated with the soft x-ray emission. The five chord system for spatially resolved intensity measurements also show these fluctuations but primarily in one line of sight, indicating that the effect is also poloidally localized.

With the electron temperatures around 100 eV, the soft x-ray emission has $h\nu \gg T_e$ and an even stronger electron temperature dependence than stated in equation 1. The oscillations in soft x-ray emission are therefore caused by a lower level of electron temperature fluctuations than what was originally assumed. The loss in electron energy content because of the fluctuations is probably of the level of a few percent.

There is, however, a larger but slower change in electron temperature, associated with the fluctuations. About 1 ms after the fluctuations appear, both in the center and at the edge, there is a 30% drop in electron temperature and a consequently decrease in energy confinement time.

My experimental contribution to this paper is the electron temperature measurement.

5.6 Paper VI

Data consistency is an important issue but holds a background position. There might seem that there is little to gain with such an investigation, either the measurement is OK, "as it should", or the error bars are too great for the data to be interesting[1].

Spectroscopic measurements, e.g. electron temperature from line ratios or ion density measurements from spectral line emission, are sometimes not taken seriously. The point of view is that there are too many assumptions in the calculations and difficulties in the measurement to make the final result reliable.

At EXTRAP-T2 we are partly depending on these measurements. Spectral line ratios in O^{5+}, measured with the VUV spectrometer, is the only time-resolved measurement of the electron temperature we have. Z_{eff} from visible bremsstrahlung give unphysically high values except at high electron densities. Instead Z_{eff} is calculated by summing the contributions from the different ionization stages of carbon and oxygen. The lower ionization stages may be calculated directly from line emission of resonant transitions but the higher, e.g. the densities of helium-like carbon and oxygen are calculated from the lithium-like densities through an ionization balance. To make the calculation more difficult, it includes the particle confinement time, a quantity which is difficult to measure accurately. As the density of C^{4+} is also calculated from a UV, near-visible transition it is possible to compare the result with the VUV measurement and use this as a consistency check of the measurements.

The comparison shows that on average the calculation based on UV line emission gives about 30% higher C^{4+} ion density than the VUV measurement. This is a pleasing result, intensity measurements are difficult and a factor of two between the two measurements would still be regarded as a good result. Even more interesting is that the difference between the UV and VUV measurement is removed completely, on average, by assuming a 20% higher electron temperature. The excitation energy for the UV transition is much higher than the electron temperature, and therefore the excitation rate coefficient is strongly dependent on the temperature. The increase in electron temperature is within the error bars of the measurement.

In the paper it is pointed out that the same result can be obtained by

[1]Someone said, although in a different context, if you have one watch you know what time it is, if you have two you only know how much they differ.

increasing the ion density of C^{3+} and/or increasing the particle confinement time. However, the electron temperature alone can explain the discrepancy, and that within error bars, neither the C^{3+} ion density nor the particle confinement time can do this. It is possible that a combination of them would be more correct, and the scatter in the data also indicates that increasing the electron temperature with 20% does not completely solve the problem. However, it removes the systematic difference between the two measurements.

Two important conclusions can be drawn from the investigation. First, we can trust the spectroscopic measurements. Second, it is possible to calculate ion densities from UV, near-visible line emission. This is an experimentally great simplification from performing measurements in the VUV wavelength region.

5.7 Paper VII

The aim of this paper was to report on changes in the intensity in the components of the Rydberg series in Cl^{16+} measured in JET plasmas. In connection with a rebuild, that effectively moved the line of sight of the Bragg crystal spectrometer from being nearly centered to almost touching the inner wall, the 1s – 10p transition in the Cl^{16+} was clearly enhanced in comparison with the other components of the Rydberg series. The line shape of the 1s – 10p transition was also changed, it is best described with a two-Gaussian profile, one hot part with the same temperature as the other components of the Rydberg series and a cold part representing emission originating from the edge. The state-selective behaviour and the low temperature of the extra component indicates that the enhancement is caused by charge exchange collisions between fully stripped chlorine and thermal background neutral deuterium at the plasma edge.

Other sources of excitation or emission, such as radiative recombination and blending lines, are investigated. The analysis of the radiative recombination and cascading from higher levels was performed with the ADAS[2] data and software package [46]. The paper also tries to give an explanation why only one level (n=10) is being populated whereas almost all charges, especially higher ones, involve more than one level. An explanation is sug-

[2]Atomic Data and Analysis Structure contains atomic data and programs to investigate atomic physic processes in plasmas. Managed by the University of Strathclyde, Glasgow, Scotland.

gested, that it appears that Z=17 is very close to resonance with a single level (n=10) in low-energy charge exchange collisions. Comparison with a similar study on charge exchange contribution to the Rydberg series in Ar^{16+} is also presented.

My contribution to this paper, as far as the analysis is concerned, is primarily of the explanation of charge exchange part of the chlorine spectrum and the differences with respect to the study on argon. Included in this is the investigation of the other sources of radiation that might have caused the observed spectra, e.g. radiative recombination and blending lines.

Chapter 6

Conclusions and future plans

The subject of this thesis is quantitative spectroscopy and its application to fusion plasma physics. The measurements are mainly of the electron temperature and impurity ion densities. They have, except for one part, been performed at EXTRAP-T2, which is a reversed-field pinch operated with a resistive shell and a graphite wall.

The resistive shell gives rise to so-called wall-locked modes which are stationary magnetic field perturbations. A significant amount of energy and particles are lost to the wall at the position of the locking and it leads to a local heating of the wall and subsequently large influxes of hydrogen and impurities. These influxes and their effect on global plasma performance have been investigated. Spectroscopic measurements show that the released impurities are mainly carbon, but also oxygen. The strong increase in electron density and impurity content leads to lower electron temperature, higher Z_{eff} and a more resistive plasma. The plasma recovers somewhat after the influx but remains in a clean but cold and resistive state.

Wall-locked modes and plasma-wall interaction manifest themselves also on the local scale. Hydrogen is released from the wall in minor influx events which do not show on the global electron density measurement. Spectroscopic measurements near the position of the influx event show strong increase in line emission originating from charge exchange collisions. This has been used to estimate the change in the neutral hydrogen density profile.

Strong temporal correlation has been observed between amplitude oscillations in soft x-ray emission from the center and poloidal loop voltage at the edge at the position of the locked modes. The fluctuation in toroidal magnetic flux is interpreted as local dynamo activity at the position of the

wall-locked mode. Linked to these oscillations is a decrease in the central electron temperature indicating that a loss channel exists at the position of the wall-locked modes, removing energy from the center and depositing it at the plasma edge.

The effect of operating with a graphite wall is that it controls the plasma density through hydrogen recycling. The graphite is a great reservoir of trapped hydrogen and several models have been tested to understand and predict the evolution of the plasma density, if not controlling it. Hydrogen recycling and loading of the wall has been investigated in an isotope exchange experiment. The ratio of the density of the hydrogen isotopes was measured spectroscopically and was found to agree well with the most sophisticated model used.

The spectroscopic measurements and models have been the subject themselves in a consistency investigation. Every aspect of electron and ion density measurement was included. Comparison of two different measurement of the ion density of C^{4+} show remarkably consistent results. The difference between the result from the two measurements can be explained with the uncertainty of the electron temperature.

Finally, contributions of charge exchange excitation to the spectrum of hydrogen-like chlorine have been reported. The key point is that only one n-level seems to be populated after the charge exchange collision between fully stripped chlorine and neutral deuterium in the ground state. This is different from most other ions. It is suggested that it is caused by the near-resonance condition in the specific collision and may serve as a test for models aimed at calculating the charge exchange collision cross-section for various charges.

Partly as a consequence of the result from the studies on EXTRAP-T2, the experiment will be rebuild. The new version of EXTRAP-T2 will resume operation sometime during the spring 2000. It will be a quite different experiment although the objective is the same, to study the effects of operating a reversed-field pinch with a resistive shell. The difference is that the shell time will be longer and that the RFP configuration will have time to establish itself before the wall-locked modes (will they be wall-locked?) will grow strong. Hopefully this will prevent them from growing at all and perhaps we will see the improvement in confinement as was suggested in paper IV.

The graphite wall will also be gone, hopefully resulting in a better control

over the plasma density. In all, the rebuilt machine should perform better and with more control.

Together with these improvements, the new machine will be better diagnosed, both in terms of magnetic and spectroscopic measurements. In connection to the work presented in this thesis there are a couple of things that is interesting to try.

I believe that it is worth the trouble to go over the visible bremsstrahlung measurement again. The upgraded machine will have sections of parallel vertical ports, with positions from the center and outwards. It might be possible to subtract the bremsstrahlung emission measured in the outermost chord from the central one and thereby remove the background emission of weak spectral lines. Comparison with VUV measurements will tell if this is working or not.

The calculation of the power balance presented in chapter 4.3 showed how crucial it is to know the electron temperature profile, especially at the edge where the greatest gradient is. One way to obtain the electron temperature profile and also potentially the electron density profile is spectral line ratios in helium. A small (non-perturbing) helium beam crossed by viewing chords for spectrometers will give a local measurement of the signal in the point of intersection. By choosing different line ratios, electron temperature and density may be determined. Potentially the system could also be applied to ion temperature and poloidal rotation through charge exchange collisions between helium and fully stripped carbon.

One final remark. In every calculation, based on spectroscopic measurements, that includes the the electron temperature, e.g. when rate-coefficients are used, the electrons are assumed to have a Maxwellian velocity distribution. It is therefore of great importance to know that this is really true. There exists super-thermal electrons in an RFP discharge and especially in the turbulent start-up phase. At the same time we observe spectral line emission from highly charged ions long before these ion would even exist at the temperatures we measure. In the main part of the discharge where the plasma current has reach its maximum almost all spectroscopic data are well described by a Maxwellian distribution. However, it is possible that a tail of high energy electrons still exists. For atomic processes that require energies in the range of the electron temperature, the bulk of the velocity distribution will do. On the other hand, processes that require energies exceeding the electron temperature will be more influenced by such a tail. It is therefore possible that the excess in light measured in the C^{5+} 5290

Å transition (paper II and section 5.5) is caused by underestimation of the rate-coefficient and that it is primarily a high energy-tail that causes the excitation. An investigation of the velocity distribution would not only increase the certainty of many spectroscopic measurements but also possibly explain a number of phenomena that are currently not understood.

References

[1] J. D. Lawson. *Proc. Roy. Soc. B*, **70**, 6 (1957).

[2] S. Craxton, R. L. McCrory, and J. M. Soures. *Sci. Am.*, **255**, 60 (1986).

[3] J. Lindl. *Phys. Plasmas*, **2**, 3933 (1995).

[4] F. F. Chen. *Introduction to plasma physics.* Plenum Press, New York (1984).

[5] J. Hedin. *Cyclotron resonance heating in toroidal plasmas.* Licentiate thesis, Royal Institute of Technology, Stockholm, 1999.

[6] G. Hedin. *Dynamo modes in reversed-field pinch plasmas with conducting and resistive shells.* PhD thesis, Royal Institute of Technology, Stockholm, 1998.

[7] J. Wesson. *Tokamaks.* Clarendon Press, Oxford (1987).

[8] J. Carlsson. *Ion cyclotron resonance heating and current drive in tokamaks.* PhD thesis, Royal Institute of Technology, Stockholm, 1998.

[9] C. Alejaldre. *Physics World*, **Oct**, 25 (1996).

[10] G. Grieger, C. Beidler, E. Harmeyer, W. Lotz, J. Kisslinger, P. Merkel, Nuhrenberg, F. Rau, E. Strumberger, and H. Wobig. *Fus. Technol.*, **21**, 1767 (1992).

[11] H. A. B. Bodin. *Nucl. Fusion*, **30**, 1717 (1990).

[12] J. B. Taylor. *Phys. Rev. Lett.*, **33**, 1139 (1974).

[13] J. C. Sprott. *Phys. Plasmas*, **31**, 2266 (1988).

[14] A. B. Rechester and M. N. Rosenbluth. *Phys. Rev. Lett.*, **40**, 38 (1978).

[15] M. R. Stoneking, S. A. Hokin, S. C. Prager, G. Fiksel, H. Ji, and D. J. Den Hartog. *Phys. Rev. Lett.*, **73**, 549 (1994).

[16] R. N. Dexter, D. Kerst, T. W. Lovell, S. C. Prager, and J. C. Sprott. *Fus. Technol.*, **19**, 131 (1991).

[17] RFX team. In *Proc. of the 14th International conf. on fusion energy organized by the IAEA, Würzburg*, volume 2, page 583, Vienna. The International Atomic Energy Agency (1992).

[18] Y. Yagi, H. Sakakita, T. Shimada, K. Hayase, Y. Hirano, I. Hirota, S. Kiyama, H. K. Y. Maejima, T. Osakabe, Y. Sato, S. Sekine, and K. Sugisaki. *Plasma Phys. Contr. Fusion*, **41**, 255 (1999).

[19] J. R. Drake, H. Bergsåker, P. R. Brunsell, J. H. Brzozowski, T. Fall, E. Gerhard, G. Hedin, A. Hedqvist, G. Hellblom, S. Hokin, P. Hörling, D. Larsson, A. Möller, E. Rachlew-Källne, J. Sallander, M. Tendler, E. Tennfors, and A. Welander. In *Proc. of the 16th International conf. on fusion energy organized by the IAEA, Montreal*, volume 2, page 193, Vienna. The International Atomic Energy Agency (1996).

[20] G. Hedin. *Plasma Phys. Contr. Fusion*, **40**, 1529 (1998).

[21] W. Engelhardt. In *Proc. Course on Diagnostics for Fusion Reactor Conditions, Varenna, Italy*, volume I, page 11, Brussels. Commission of the European Communities, EUR 8351-I EN (1982).

[22] H. R. Griem. *Plasma Spectroscopy.* Cambridge University Press (1997).

[23] J. Z. Klose and W. L. Wiese. *J. Quant. Spectrosc. Radiat. Transfer*, **42**, 337 (1989).

[24] C. F. Maggi. *Measurement and Interpretation of Spectral Emission from JET Divertor Plasmas.* PhD thesis, University of Strathclyde, 1996.

[25] H. R. Griem. *Plasma Spectroscopy.* McGraw-Hill (1964).

[26] R. R. Goforth, T. N. Carlstrom, B. Curwen, et al. *Nucl. Fusion*, **26**, 515 (1986).

[27] D. Larsson. *Surface processes and wall conditioning in fusion experiments.* PhD thesis, Royal Institute of Technology, Stockholm, 1998.

[28] A. Welander. *An experimental investigation of electron confinement in reversed-field pinches.* PhD thesis, Royal Institute of Technology, Stockholm, 1998.

[29] R. J. Fonck, A. T. Ramsey, and R. V. Yelle. *Appl. Opt.*, **21**, 2115 (1982).

[30] J. S. Haskovec, G. Bramson, N. H. Brooks, and M. Perry. In *Proc. of the 13th Symp. on Fusion Eng, Knoxville, TN*, volume 1, page 153, New York. Institute of Electrical and Electronics Engineers (1990).

[31] L. Carraro, M. E. Puiatti, P. Scarin, and M. Valisa. *Rev. Sci. Instrum.*, **63**, 5188 (1992).

[32] J. Sallander. *Rev. Sci. Instrum.*, **69**, 2357 (1998).

[33] J. Jacquinot and JET team. *Nucl. Fusion*, **38**, 1263 (1998).

[34] P. Thomas et al. *Phys. Rev. Lett.*, **80**, 5548 (1998).

[35] R. J. Hawryluk et al. *Phys. Plasmas*, **5**, 1577 (1998).

[36] R. Bartiromo, F. Bombarda, R. Giannella, S. Mantovani, L. Panaccione, and G. Pizzicaroli. *Rev. Sci. Instrum.*, **60**, 237 (1989).

[37] K. Kadota, M. Otsuka, and J. Fujita. *Nucl. Fusion*, **20**, 209 (1980).

[38] W. J. Karzas and R. Latter. *Astrophys. J.*, **6**, 167 (1961).

[39] A. T. Ramsey. *Rev. Sci. Instrum.*, **58**, 1211 (1987).

[40] I. H. Hutchinson. *Principles of plasma diagnostics.* Cambridge University Press, Cambridge (1987).

[41] N. Schoon, J. Ongena, G. Van Oost, J. Schwartz, G. Telesca, and A. Cosler. *Measurement of the bremsstrahlung radiation in the visible and determination of Z_{eff} on TEXTOR.* Technical Report 92, TEXTOR, 1990.

[42] K.-D. Zastrow. *Quantitative Plasma Spectroscopy at JET and Extrap-T1.* PhD thesis, Royal Institute of Technology, Stockholm, 1993.

[43] L. Spitzer. *Physics of fully ionized gases.* Interscience, New York (1962).

[44] J. Sallander. *Plasma Phys. Contr. Fusion*, **41**, 679 (1999).

[45] P. Nordlund and S. Mazur. *Phys. Plasmas*, **1**, 4032 (1994).

[46] H. P. Summers. *Atomic Data and Analysis Structure.* Technical Report JET-IR(94)-06, Jet Joint Undertaking Report, 1994.